ISSN 0469-4732

INSTITUTE OF PLASMA PHYSICS

NAGOYA UNIVERSITY

Study of Critical Beta Non-Circular Tokamak Equilibria Sustained in Steady State by Beam Driven Currents

K. OKANO, Y. OGAWA and H. NAITOU

(Received — July 5, 1988)

IPPJ- 878 July, 1988

RESEARCH REPORT

NAGOYA, JAPAN

STUDY OF CRITICAL BETA NON-CIRCULAR TOKAMAK EQUILIBRIA SUSTAINED IN STEADY STATE BY BEAM DRIVEN CURRENTS

K. OKANO*, Y. OGAWA and H. NAITOU

(Received - July 5 , 1988)

IPPJ- 878 July 1988

Further communication about this report is to be sent to the Research Information Center, Institute of Plasma Physics, Nagoya University, Nagoya 464-01, Japan

---

* Permanent address: TOSHIBA Research and Development Center, 4-1, Ukishima-cho, Kawasaki 210, Japan.

ABSTRACT

A new MHD-equilibrium/current-drive analysis code was developed to analyse the high beta tokamak equilibria consistent with the beam driven current profiles. In this new code, the critical beta equilibrium, which is stable against the ballooning mode, the kink mode and the Mercier mode, is determined first using MHD equilibrium and stability analysis codes (EQLAUS/ERATO). Then, the current drive parameters and the plasma parameters, required to sustain this critical beta equilibrium, are determined by iterative calculations. The beam driven current profiles are evaluated by the Fokker-Planck calculations on individual flux surfaces, where the toroidal effects on the beam ion and plasma electron trajectories are considered. The pressure calculation takes into account the beam ion and fast alpha components. A peculiarity of our new method is that the obtained solution is not only consistent with the MHD equilibrium but also consistent with the critical beta limit conditions, in the current profile and the pressure profile. Using this new method, β ~21% bean and β ~6% D-type critical beta equilibria were scanned for various parameters; the major radius, magnetic field, temperature, injection energy, etc. It was found that the achievable Q value for the bean type was always about 30% larger than for the D-type cases, where Q=fusion power/beam power. With strong beanness, Q~6 for DEMO type tokamaks (~500 MWth) and Q~20 for power reactor size (4.5 GWth) are achievable. On the other hand, the Q value would not exceed sixteen for the D-type machines.

1. INTRODUCTION

A steady state tokamak should be an attracttive candidate as future power reactor, if its current drive power is at an acceptable level. On the other hand, high beta tokamak operation will be indispensable for a power reactor, from an economical point of view. A common result from the present theoretical and experimental high beta studies is that high plasma currents are inescapably required in high beta operations. Namely, with plasma current I_p, cross-section half width of the plasma on the equatorial plane, a, and toroidal magnetic field, B_t, the achievable maximum value of toroidal beta β_{cr} [1,2,12] is given by

$$\beta_{cr}[\%] = g \cdot \frac{I_p[MA]}{a[m]\ B_t[Tesla]}, \qquad (1)$$

where g is nearly constant at about 3 but weakly depends on the aspect ratio and the plasma shape [2]. The fact that a high beta operation bounds up with a large plasma current should be undesirable from the viewpoint of current drive for steady state tokamaks, because a larger current requires a larger drive power. This problem regarding the high beta steady state tokamaks was discussed earlier in Ref.[11].

It is useful to review the parameter dependence of energy gain Q in order to clearly understand the relationship between high beta and steady state operations. With a retained plasma temperature, we can regard as $\beta_t \propto n_e$ and the thermo-nuclear power $P_f \propto n_e^2 \propto \beta_t^2$, where the electron density n_e is regarded as being proportional to fuel ion density n_i. Considering that I_p and the current drive efficiency are proportional to β_t[by Eq.(1)] and n_e^{-1}, respectively, the required power to drive the currents, P_{dr}, is related as $P_{dr} \propto I_p \cdot n_e \propto \beta_t^2$. Namely, we can conclude that the energy gain $Q=P_f/P_{dr}$ does not change by increasing β_{cr}, if the factor g in Eq.(1) is absolutely constant. Moreover, the higher beta results in a drive power increment proportional to β_t^2. Even by this very rough calculation, it was clarified that the relationships between high beta MHD stability and the current drive parameters are important for steady state tokamak analysis. The parameter study

on steady state tokamaks would be worthless, without any consideration of the driver power required from the beta limit and the stable limit on q_* etc.

The main aim of this study was to investigate the above problem in detail in regard to steady state tokamaks over the Ref.[11]. It is well known that the conditions for global parameters, for example I_p, B_t etc., are insufficient to allow disscussing the critical beta equilibria. Rather, the profiles (for density, temperature etc.) in plasmas play an important role. On the other hand, the current drive characteristics also depend on the profiles, and the driven current profiles would be unsuitable to sustain the critical beta equilibria without any current profile control. Therefore, for a strict analysis on steady state tokamaks, the pressure profile and the current profile should be treated at a same time without any inconsistency with MHD equiribrium, stability and the current drive parameters. The previous work [11] lacked such a microscopic treatment on the profiles, where the g-value[Eq.(1)] and the driven current had been conditioned using Yamazaki, et al. type (modified Troyon type) beta limit scaling[2].

In this study, the authors investigated the performance of the steady state tokamaks, without the above inconsistency, by combining a 2-D MHD equilibrium code (EQLAUS[13,15]), a 2-D MHD stability analysis code(ERATO[13,14,15]) and a 3-D beam current drive analysis code[5], based on Mikkelsen and Singer's model [3]. The global energy confinement times, to sustain these tokamak equilibria, were also checked by Kaye-Goldstone type energy confinement scaling[27].

The neutral beam current drive (NBCD) has been chosen here. This method was theoreticaly prospected by Ohkawa in 1970[4]. In tokamak experiments, after the early NBCD experiment with DITE[6], large driven currents of near half-mega amperes have been observed in recent NBCD experiments with JET[28] and TFTR[29]. The flexible current profile controllability by NBCD has been also predicted by numerical simulations[5]. Besides, most of the present high beta tokamak experiments have been accomplished with neutral beam heating. Considering these results and the fact that the present NBCD theory has shown

good agreement with the experimental values[7], the beam current driver seems to be most reliable in compatibility with high beta operations, and is a logical choice for the present purpose.

The authors' main interest, in this study, is to reconfirm the Q-enhancement effect by strong plasma shaping, which has been proposed in Ref.[11]. This effect comes from a g-increment by bean shaping, where g is the factor in Eq.(1). Thus, strongly indented bean shaped plasmas are considered here, but conventional D-type plasmas were also investigated for reference. The DEMO class with several hundred MWth thermal output and the power reactor grade with several GWth are considered as the machine sizes. Many parameter scans were made with various R_0(major radius), plasma temperatures, and toroidal field strengths, etc. Merits and weaknesses are disscussed in regard to the bean type tokamaks versus the D-types. Beam energy were also scanned, up to 2 MeV. It is shown that the optimized beam energies are somewhat lower than the results reported in the previous paper[5], where the near parabolic driven current profile has been chosen without any MHD equilibrium calculations.

In the early technique for a consistent analysis of MHD equilibrium and current drive, the plasma pressure profile was determined for the driven current profile by iterative equilibrium/current drive calculations. The authors named this method the 'forward solution'. The first valuable work citing the forward solution was accomplished by Ehst et al.[8,9], where the r.f. current driver was chosen. The authors'previous work on high beta tokamaks with NBCD was also made according to the forward solution[35]. Another example of the forward solution is given in Ref.[10].

In the forward solution, the current driver parameter are determined first. Therefore, the final converged equilibrium will not satisfy the marginally stable critical beta conditions given by the MHD analysis for the kink and balooning mode. Then, in order to find one of

the beam driven critical beta equilibria, the beam driver parameters must be scanned by trial and error. Such a method is unsuitable for the present purpose, i.e. wide range parameter scans for R_0, B_t, T_e, beam energy E_b, plasma shapes, etc.

The authors developed a new method to overcome the above difficulty of the forward solution. In this method, the alternating calculations, between MHD equilibrium/stability and current drive, can be eliminated. First of all, a marginally stable MHD equilibrium, against ballooning, kink and Mercier modes, is determined by EQLAUS/ERATO iterative calculations[15]. Then, the optimized current profile $j(\psi)$, the pressure profile $p(\psi)$ for the beta limit and other equilibrium data are transfered to the NBCD analysis code (DRIVER[5]). Next, the beam power distribution in the beam transmission line (or neutralizer outlet) and the fuel ion density profile are determined by iterative current drive and total presure calculations, so that the current profile and the pressure profile, composed of thermal,beam and α-particle pressures, can be strictly the same as the EQLAUS/ERATO calculation. The flexible current profile controllability by NBCD[5] makes such current profile tailoring possible. The beam design, optimized to sustain the critical beta equilibrium, is obtained by this new method, and the optimized solution gives various figures of merits (current drive efficiency, shinethrough, Q-value etc.).

Using this method, named the 'reverse solution', the parameter scan is possible for beam energy, plasma temperature, etc. without any recalculation of equilibrium, once a critical beta equilibrium is obtained from EQLAUS/ERATO calculations. Furthermore, as the equilibrium is normalized in the EQLAUS/ERATO code, R_0 and B_t scans are also possible,while retaining the scaling parameters (I_p/R_0B_t, R_0/a, β, parameter profiles etc.). All the present results of this study were obtained by this efficient 'reverse solution' method. Namely, all the calculations are strictly consistent with the critical beta equilibria.

This paper contains the following. In the next section, an overview

of the beam current drive analysis code is given. An outline of the MHD equilibrium/stability analysis code is reviewed in Section 3. Some example of critical beta equilibria, used in the reverse solution, are shown in Section 4. The results obtained from parameter scans are described in Section 5 for the DEMO class machines and in Section 6 for the power reactor grade cases. Some noteworthy problems are discussed in Section 7 and the summary is given in the final section.

2. BEAM CURRENT DRIVE ANALYSIS

2.1 Code Outline

The beam current drive analysis code system (DRIVER) is composed of a 3-D beam power & momentum deposition code and a 2-D Fokker-Planck calculation code. Various plasma shapes, include D- and bean types, can be treated in both codes. The injection beam can be asymmetric with regard to the equatorial plane, and the beam line can be tilted by θ_v from the horizontal plane [Fig.1]. Beam divergence can also be taken into acount, while no divergence was assumed in this study, because the beam divergence is usually small for high energy beams[23].

The beam cross-section shape is given by input data. This beam is split into many (maximum 200) fine beamlets and the power distribution in the beam line, $P_{inj}(z)$ (see Fig.1), is modelled by the individual beamlet powers. The power and momentum deposition is calculated by further splitting each beamlet into finite pencil beams. Ionization processes are calculated along each pencil beam within a maximum of 1000 times. The total ionization events, calculated for all beamlets, are over 10^5 times. The present calculation includes the ionization cross-section by impurity species. Details are described in Ref.[5].

In order to take into account the driven current reduction by the trapped ion trajectories, when the first cycle of fast ion trajectory is of trapped, the deposited momentum in each event is set to zero, while its deposited power is made to remain. With this treatment, the driven current reduction, due to the direct trapping effect, can be included in the present model. Althouth most tangentially injected beam ions fall into the passing orbit region in the velocity space, these passing ions can be diffused into the trapped orbit region by pitch angle diffusion during the slow down process. This effect is missed in the present model, because the non-bounce average Fokker-Planck equation is used in order to reduce the computation time (the F-P equation must be solved over 10^3 times to obtain a final converged solution).

Such a large pitch angle diffusion, however, occurs in the velocity regime $v<<v_c$ (v_c:critical velocity [3], $v_c=1.42\times10^6(m/s)(\bar{T}_e/keV)^{0.5}$), while the injection velocity for the beam current drive is usually much larger than v_c. Therefore, the current reduction by this diffusion into the trapped region would be small, especially for the deeply tangential injected beams considered here.

The plasma poloidal cross-section is split into 100 flux surfaces as the numerical mesh in the real space for these calculations. The spatial steps, Δr, for the flux surface half width between individual flux surfaces and their neighbors, are taken to be constant. In EQLAUS/ERATO codes, the flux surfaces for the ψ-space mesh are chosen [see Fig.2]. This ψ mesh is converted to the equi-Δr mesh for the DRIVER code. The flux surfaces are relabeled by r in real space, instead of $s=(\psi/\psi_a)^{1/2}$ in ψ space. The physical meaning of r is the half width of the flux surface on the equatorial plane. An example of an equi-Δr mesh is found in Fig.3, where only 10 flux surfaces are shown, while 100 flux surfaces are used in the code. The flux surface average driven current-density for the beamlet No.L, between flux surfaces k and k-1, are given as follows in the DRIVER code[5]:

$$\langle j_L \rangle_k = \langle j_t/p_d \rangle_k \cdot \langle p_d \xi_b \rangle_k \qquad (2)$$

where the $\langle j_t/p_d \rangle_k$ values are determined for individual flux surfaces by the Fokker-Planck calculations[3,18], which include the toroidal effects on the return electron currents[20]. The charge exchange ion loss can be taken into account[19], but no charge exchange loss was assumed in this study. The energy diffusion, during the beam ion slowing down, is approximetely included in the present model[5]. The $\langle p_d \xi_b \rangle_k$ values are defined as

$$\langle p_d \xi_b \rangle_k = \Sigma(\Delta P_d \xi_b)/V_k \qquad (3)$$

where V_k is the volume surrounded by flux surfaces k and k-1. The pencil beam deposition powers ΔP_d, between the flux surfaces k and k-1, and the beam ion pitch angles ξ_b, at indivisual damping points, are evaluated for individual ionization events along the pencil beams. The summation is taken over all ionization events occured between the flux surfaces k and k-1.

The driven currents are calculated for the indivisual beamlets. Using the current density driven by beamlet No.L ,$\langle j_L \rangle_k$, the total current density $\langle j_t \rangle_k$ is given by

$$\langle j_t \rangle_k = \sum_{L=1}^{N} \langle j_L \rangle_k. \qquad (4)$$

As the power for beamlet No.L, P_L, is linearly proportional to $\langle j_L \rangle_k$, the current density for any new P_L is simply given by $\langle j_L \rangle_{k\ NEW} = \{\langle j_L \rangle_k / P_L\} \cdot P_{L\ NEW}$, once $\langle j_L \rangle_k / P_L$ (L=1,2,$\cdots$L) are obtained. This property is repeatedly used for current profile tailoring in each convergence loop in the reverse solution. Note that this relation is unavailable, when background plasma parameters, like the density profile, have been changed. The total pressure convergence method in the reverse solution, where the density is iteratively changed, is described later.

2.2 Current Profile Control

The driven current profile changes with the beam injection parameters. Considering a square cross-section beam with height h and width w, the minimum major radius of the beam center line is expressed as R_{tang}, the vertical angle from the equatorial plane as θ_v, and the beam center line shift, at the beam entrance where $R=R_0+a$, as Z_h. An example of a beam line for $Z_h=0$ is shown in Fig.1.

When $Z_h=0$, $\theta_v=0$ and $R_{tang}<R_0$, the beam line passes the plasma center. The current driven by such a beam is usually very peaked at the center. If $Z_h>h/2$, the beam line misses the plasma center and the driven current should be intrinsically hollow. In the same way, if $R_{tang}>R_0+w/2$, the current profile should be hollow. Its current peak position would change with Z_h, R_{tang} and θ_v. Therefore, current profile tailoring is possible by using multi-beam lines with various Z_h and/or θ_v values[5,7,21] or with various R_{tang} values[22] and by controlling each beam line power. It is also proposed to control the current profile by a high h/w ratio rectangular beam with a controlled power distribution[10]. In this study, the authors are considering this last method. The beam power distributions were modeled by many beamlets with variable powers. The final solutions will give the beam power distributions $P_{inj}(Z)$ [Fig.1] to sustain the critical beta equilibria determined by the MHD equilibrium/stability analysis.

To obtain the reverse solution, the DRIVER code controls the power for each beamlet, so that the driven profile deviation from the profile, determined from the critical beta equilibrium, can be as small as possible. Of course, it is possible that the objective current profile, given by EQLAUS/ERATO, may not be reproduced by beamlet power control only. For example, centrally localized current profiles cannot be driven in a high density plasma, because the beam power intrinsically deposits in the plasma outside. Fortunately, the present optimized current profiles were achieved by beamlet power control, when some suitable R_{tang} and beam line height were assumed.

A large beam height and $R_{tang} < R_0$ are basically preferable.

3. MHD EQUILIBRIUM AND STABILITY ANALYSIS

3.1 Equilibrium Code(EQLAUS)

The MHD equilibrium analysis code EQLAUS was developed by Gruber et al [13]. In this study, the converted version for IPPJ, which was modified to treat the indented shape plasma, has been used[15]. The EQLAUS code is linked to ERATO, which will be described later.

The two dimensional MHD equilibrium equation (Grad-Shafranov equation) is solved by EQLAUS in a (R, ψ, Z) cylindrical co-ordinate system[16].

In the present EQLAUS code, the plasma shape, including the bean type, is given as a fixed boundary;

$$R_0 = R_0 + a(\cos\theta - \delta \cdot \sqrt[\lambda]{\sin^2\theta}\ ) \tag{5}$$

$$Z = \pm \kappa a \cdot \sqrt[\lambda]{|\sin\theta|} \tag{6}$$

where a is the plasma width on the equatorial plane, and κ and δ are the plasma elongation and triangularity, respectively. The factor λ is a constant used to characterize the plasma shape ($\lambda=1, \delta<0.5$; D-shape, $\lambda=1, \delta>0.5$; Crescent, $\lambda=2$, $\delta>0$; Rounded bean)[2,15].

3.2 MHD Stability Code (ERATO)

The ERATO IPPJ version, which was also modified to treat the bean shape plasma [15], analyses the $n=\infty$ ballooning mode stability by the ballooning equation[17] as well as the n=1 kink mode stability. The Mercier mode criteria are also checked to cover the accuracy deterioration of the ballooning equation near the magnetic axis[13].

The optimized equilibria used in this study satisfy the stable conditions in regard to the n=1 kink mode, the $n=\infty$ ballooning mode and the Mercier mode. These equilibria have been obtained by the optimization of I_p, pressure and their profiles, $j(\psi)$ and $p(\psi)$, by a wide range parameter scan[15].

A finite ψ-χ mesh (60×30) was used for the present ERATO calculations, where χ is the poloidal angle. When the normalized eigenvalue, γ^2, is less than 10^{-4}, the plasma is regarded as being stabilized. This is

because such a small γ^2 is expected to converge to zero with an infinite number of meshes.

The beta limits, given by the present critical beta equilibria, are lower than the results given by the optimization for the ballooning and Mercier mode only[2], because the kink mode stability condition usually gives the lowest beta limit. An ideal conducting shell is assumed in the bean case calculations, because a conductive shell is effective in stabilizing the kink mode for bean type plasma. The conducting shell position $\rho_w(\chi)$ is given by $\rho_w(\chi) = \rho_p(\chi) + (R_{EXT}-1)\{\rho_p(0)+\rho_p(\pi)\}/2$, where ρ_p and ρ_w are the distances to the plasma surface and to the shell from the magnetic axis, respectively. $R_{EXT}=2.0$ for bean type and $R_{EXT}=\infty$ for D-type are used.

The present critical beta equilibria are based on the following tacit conditions: First, the central q value $q_0 \sim 1$. Second, the q value monotonically increases outward and on the plasma surface, $q_s \geqq 2$. Third, only the first stability regime for the ideal mode is considered. The first two condition are imposed considering the resistive mode stability condition. The last one is a logical choice, because no experimental verification of the second stability has been obtained to date. The critical beta equilibria for D- and bean types are shown in Fig.2. The plasma parameter details are described later.

3.3 Treatment for Reverse Solution Convergence.

(a) Current profile convergence.

The theory for MHD equilibria generated by r.f. driven currents was developed by Ehst[8]. The authors have used his method with a small modification for NBCD.

The current profile, which is given by the Fokker-Planck calculations, is the flux-surface average current-density $\langle j_t \rangle$ [Eq.(4)]. On the other hand, the current density $j_\phi(R, \psi\ Z)$, which is obtained by the Grad-Shafranov equation, includes the Pfrish-Schlüter current[8,24]. Therefore, the current j_{ext}, to be driven externally by a non-inductive current driver, is different from j_ϕ. Ehst derived the expression of j_{ext} as follows:

$$j_{ext} = \frac{\langle j_\parallel B \rangle}{\langle B^2 \rangle} B \tag{7}$$

where $j_\parallel$ is the current along $\vec{B}$ and $B=|\vec{B}|$. The brackets $\langle\ \rangle$ mean the following average:

$$\langle f \rangle = \int f B_p^{-1} dl \Big/ \int B_p^{-1} dl \tag{8}$$

where B_p is the poloidal magnetic field. The integral is carried out along the poloidal cross-section of the flux surface. Note that j_{ext} is not constant on the flux surface, but is proportional to B. As the circulating beam ions can be regarded to lie parallel to the magnetic field, the beam driven current density j_{bt} is also proportional to B. Namely, the local driven current density is given by $j_{bt}=j_0 B/\langle B \rangle$, where j_0 is the local current density at a point where $B=\langle B \rangle$. It can easyly be confirmed that j_0 is equal to $\langle j_t \rangle$, given by Eq.(4). Finally, j_{bt} is equivalent to the equilibrium current profile j_{ext}, when $\langle j_t \rangle$ satisfies the following relation:

$$\langle j_t \rangle = \langle j_{ext} \rangle \equiv \frac{\langle j_\parallel B \rangle}{\langle B^2 \rangle} \langle B \rangle\ . \tag{9}$$

In the corresponding expression in Ref.[8], $\langle B \rangle$ in eq.(9) is replaced by $[B]_x$, which is the magnetic field strength at the wave damping point.
This is because, in Ref.[8], the local driven current density was given by $j_{bt}=j_x B/[B]_x$, where j_x is the current density at the damping point.

Since the r.f. wave ray deposits the power at one point (the damping point) on each flux surface, the treatment with j_z would be better for RFCD. On the other hand, in the present NBCD calculation, many pencil beams deposit their powers at various positions. In our treatement, j_0 can be regarded to be equivalent to $\Sigma j_z\langle B\rangle/[B]_z$, where the summation is taken over all ioization events on the flux surface.

The current tailoring routine in DRIVER code is always controlling the driven current profile $\langle j_t\rangle$, so as to satisfy Eq.(9), where $\langle j_t B\rangle$, $\langle B^2\rangle$ and $\langle B\rangle$ on each flux surface mesh are transferred to the DRIVER code from the EQLAUS/ERATO code.

(b) Total pressure profile convergence.

In order to obtain a beam driven equilibrium, consistent with the MHD analysis, the total pressure profile p(r) should also be equivalent to that for EQLAUS/ERATO calculation everywhere in the plasma. The total pressure p is composed of the thermal component p_{th}, the fast alpha particle component p_a and the circulating beam ion component p_{beam}:

$$p(r) = p_{th}(r) + p_a(r) + p_{beam}(r) \qquad (10)$$

where the physical meaning of r is the half width of the flux surface on the equatorial plane, but it can be regarded as the flux surface label as well as $s=(\psi/\psi_a)^{1/2}$. With the local ion and electron temperatures, T_j, T_e, and their densities, n_j, n_e, the thermal pressure $p_{th}(r)$ is given by $P_{th}(r)= n_e(r)T_e(r) + \Sigma n_j(r)T_j(r)$, where the summation on j includes all impurity ion species. The fast ion pressures by alphas(subscript a) and by beam ions(subscript b) are given on the individual flux surfaces by

$$p_{a,b} = [E_{a,b}]\dot{n}_{a,b}\,\tau_{a,b}\,, \qquad (11)$$

where [E] is the average ion energy in velocity space, $\dot{n}$ is the fast ion birth rate and τ is the fast ion thermalization time. The [E] and τ values are evaluated by the Fokker-Planck calculation. The alpha presuure p_a is composed not only of the fast alpha component due to thermo nuclear D-T

fusions, $p_{\alpha th}$, but also of the fast alpha component generated by direct beam ion reactions with thermal T^+ ions, $p_{\alpha TCT}$ (TCT effect[26]). Any D-D reactions can be neglected for the present purpose. The profiles for p_{beam} and $p_{\alpha TCT}$ change by controlling the driven current profile. In the reverse solution code, the profiles p_{beam} and p_α (= $p_{\alpha th} + p_{\alpha TCT}$) are evaluated and then the density profile is changed after the current profile tailoring so that the total pressure profile p(r) can be equivalent to the pressure profile given by the critical beta equilibrium. The calculation is repeated from the beam power deposition step, because now the background plasma has been changed. These beam deposition, current tailoring and pressure fitting processes are iterated by 15~20 times, in order to obtain the final consistent solution. During the iteration, the temperature profile is kept at

$$T(r) = T_0[\, 1-(r/a)^{\alpha_1}]^{\alpha_2} \,. \qquad (12)$$

In this study, the temperature profiles have been chosen so as to obtain near parabolic density profiles in the converged solutions.

The convergence of the reverse solution seems to be more difficult than for the forward solution process. The main reason for this difficulty comes from the density change during the iterations. As the thermal output is proportional to n_i^2, p_α can be largely modified step by step. Sometimes the calculation fell into an oscillating loop. In order to overcome this difficulty, in the first five steps, the fusion reaction rate was set to zero and the beam power was ramped up. In the next five steps, the reaction rate was also ramped up. Then, the iterations were continued till a final convergence.

In the final converged solution, errors remaining in I_p and in the volume averaged total pressure are maintaind at zero. Local error for p(r) and j(r) are less than 5% and in most cases less than 2%, except for the just edge region, where p(r)~0 and j(r)~0.

3.4 Equilibrium Scaling

The current profile j and the pressure profile p are normalized in the following forms for the EQLAUS/ERATO codes:

$$\tilde{j}(s) = \frac{\mu_0 R_x}{B_{tx}} j(s) \tag{13}$$

$$\tilde{p}(s) = \frac{\mu_0}{B_{tx}^2} p(s) \quad , \tag{14}$$

where $s=(\psi/\psi_a)^{1/2}$, R_x is the major radius of magnetic axis and B_{tx} is the magnetic field strength on the magnetic axis. The R_x value is different from the R_0 value due to the magnetic axis shift in the finite beta toroidal system. When Eqs.(13) and (14) are satisfied and the aspect ratio and the plasma shape are maintained similar, the critical beta equilibria are strictly similar for any R_x and B_{tx}. In the present study, the authors have calculated the equilibria with R_x=1.0(m), B_{tx}=1.0(Tesla). With $j_1(s)$ and $p_1(s)$ in these base equiribrium solutions, the j(s) and p(s), for various R_x and B_{tx}, are given by

$$j(s) = \frac{B_{tx}}{R_x} j_1(s) \tag{15}$$

$$p(s) = B_{tx}^2 p_1(s) \quad . \tag{16}$$

Note that R_x is not independent from B_{tx} in this scaling, because the value I_p/R_xB_t must be constant to satisfy Eq.(15). The value I_p is uniquely determined by the R_x and B_{tx} values.

Although the total pressure profile is scaled as above, those component ratios for the thermal pressure, fast alpha pressure and circulating beam ion pressure will change according to the plasma size, temperature and various other beam and plasma parameters. Therefore, the driven current and pressure calculations in DRIVER must be carried out with real (non-normalized) parameters for individual equilibria. However, no recalculation by EQLAUS/ERATO is required for the parametric scan by the present reverse solution code, when the above scaling parameters are retained. This property in the reverse solution greatly simplifies the present wide range parametric study.

4. MACHINE PARAMETERS AND CRITICAL BETA MHD EQUILIBRIA

Critical beta MHD equilibria, which are marginally stable with regard to the $n=\infty$ ballooning mode, the $n=1$ kink mode and the Mercier mode, are obtained by the optimization of $j(\psi)$ and $p(\psi)$ through the iterative EQLAUS/ERATO calculations [15,34]. The critical beta equilibria for D- ($\lambda=1$, $\delta=0.3$) and bean ($\lambda=2$, $\delta=1.5$) types, used in this study, are shown in Figs.2-a and b, respectively. Both equilibria satisfy the conditions for monotonic q-increments, $q_*(0)\sim1$ and $q_*(a)>2$. The current and pressure profiles was almost optimized and maximized in these equilibria.

The q_* value for the present bean type equilibrium, $q_*=3.22$, is much larger than the above $q_*(a)>2$ restriction. This is because a further increase in l_p, i.e. a decrease in q_*, leads to a beta limit degradation due to MHD instability.

These equilibria are normalized in the forms described in Section 3.4. All the beam generated MHD equilibria, presented in this paper, are identical to the normalized equilibria in Fig.2. The basic parameters for these critical beta equilibria are listed in Table 1. The plasma size parameters, used in the parametric scanning, are also listed in this table. The plasma sizes are cataloged by the 'plasma box major radius R_0^*', which is defined in Fig.3 with other plasma shape parameters (R_0, a, a^*, R_{min}, R_{max}, etc.). Note that these definitions are different from the notation in Ref.[2]. The plasma aspect ratio A, elongation κ and indentation i (for bean) are defined as ; $A=R_0^*/a^*$, $\kappa=b/a$ and $i=d/(R_{max}-R_{min})$. For the same R_0^*, the plasma volumes V_p for D- and bean types are nearly equal to each other (DEMO 2 and 3). The plasma major radius R_0 can be converted into the magnetic axis major radius R_x by the relations '$R_0=0.96R_x$' for the present D-type and '$R_0=0.98R_x$' for the bean type, respectively.

The neutral beam line positioning and cross-section shape parameters are summarized in Table 2. The beam line parameters differ between the D-type cases and the bean type cases. However, these parameters are similar for

different R_0 values. In Table 2, the beam line dimensional parameters are normalized by R_0. All beam line cross-sections are rectangular with height h and width w. Two types of beam lines, where one is the central current driver (No.1) and other is the edge profile shaper (No.2), are required for the bean type plasmas in order to tailor the current profile, while one type of beam line is sufficient for the D-plasmas. The beam line cross-sections at $R=R_{tan}$ are drawn in Fig.2.

In order to obtain the reverse solution, the temperature profiles $T_e(r)$ and $T_i(r)$ should be given in the form of Eq.(12). In the present study, the authors have chosen $\alpha_1=6.0$ and $\alpha_2=1.0$ for bean types, and $\alpha_1=10.0$ and $\alpha_2=1.0$ for D-types, except for the temperature profile scan in Section 5.4.
These value choices result in near parabolic density profiles in the converged solutions. The reason for these choices, where the temperature profiles are very broad, is clarified in Section 5.4. An example of density profiles in the converged solutions is shown in Fig.4 with the temperature profile, where $R_0^*=3.18$m (bean type), $\bar{T}_e=\bar{T}_i=20.7$keV, $B_{ta}=2.77$T and $E_b=600$keV.

The volume average temperature $\bar{T}_j$ are defined by

$$\bar{T}_j=\int_V n_j \cdot T_j \, dV \Big/ \int_V n_j \, dV \, . \qquad (17)$$

Therefore $\bar{T}_j$ would change slightly with a change in the density profile, even when the T_j profile is retained. However, this change is usually small (<1keV) during the iteration process.

5. PARAMETRIC SCAN FOR DEMO SIZE MACHINES

In this section, the authors discuss the results of parametric scans for DEMO size beam driven tokamaks (DEMO 1~4 in Table 1), where the fusion output is several hundred mega-watts in thermal power.

5.1 Examples of Beam Generated Critical Beta Equilibria

A beam generated critical beta equilibrium, obtained by the present reverse solution code, is shown in Fig.5, where DEMO-2 bean type (in Table 1, R_0^*=3.86m) is used with B_t=2.5T. The figures show the driven current density j (and the total current value I_p), the total and each component pressure, the beam power distribution $P_{inj}(z)$ (and the injection power value P_b) to sustain the critical beta equilibrium. Since $P_{inj}(z)$ in an unit beam line is in inverse proportion to number of the beam line units (or number of the injection ports) N_b, the beam power distribution is plotted as $N_b \cdot P_{inj}(z)$. The beam energy, E_b, is 600keV and $\bar{T}_e=\bar{T}_i$=20keV.

The converged solution gives P_f=647MW, $\bar{n}_e=0.67\times10^{20}m^{-3}$, P_b=98MW and Q=6.6 with B_t=2.5T. In the plots for j, the solid line is the beam driven current profile $j_b=\langle j_t\rangle B/\langle B\rangle$, and the broken line indicates the equilibrium current profile; $j_{ext}=\langle j_\parallel B\rangle B/\langle B^2\rangle$. The local error in j_b from j_{ext} is less than 5% in the whole range, except for just at the edge region, where j~0.

The pressure profile, p ($=p_{th}+p_{beam}+p_\alpha$), also converged on the equilibrium pressure profile. In the near edge region, where p~0, some small deviation from the equilibrium pressure profile remained in some cases, but its effect on the global parameters (Q, P_f, etc.) is negligible. Although the beam pressure is the lowest component near the plasma center, it exceeds p_{th} and p_α in the edge region, and becomes the largest component, as shown in Fig.5. This is because the current profile, required by the critical beta equilibrium, is quite broad (weakly hollow for the bean type). Therefore, considerable power should be injected into the edge region by beam No.2, in order to shape the edge current profile.

Most of the beam shinethrough occured in the No.2 beam. The shinethrough fraction for No.1 beam was very small (<<1%). The shinethrough from the low density edge region would be a weakness of the beam current driver in the high beta tokamak operations.

Another example equilibrium for the DEMO-3 D-type is shown in Fig.6, where R_0^*=4.55m, $\bar{T}_e=\bar{T}_i$=20keV and E_b=600kev. In this case, the local error in j(r) and p(r) is less than 2% except for just at the edge. The solution gives P_f=631MW, $\bar{n}_e=0.53\times10^{20}m^{-3}$, P_b=128MW and Q=4.9 with B_t=4.5T. One of differences from the bean case is that the edge region injection power can be reduced in the D-case, because the D-type critical beta equilibrium does not require a hollow current profile, as is needed in the bean cases. As a result, the shinethrough power from the low density edge was reduced.

As the beta value of D-type equilibrium (6.05%) is much smaller than the bean type beta (20.9%), the toroidal field B_t, to obtain an output the same as the bean, is nearly twice that for the D-type machine, although the plasma volume of DEMO-3 Dee is 1.8 times larger than the DEMO-2 bean, used in Fig.5.

5.2 Plasma Size and B_t Scan

The results of plasma size and B_t scan for DEMO machines (3 sizes for both bean and D, listed in Table 1) are plotted in Fig.7 as functions of the fusion output P_f, where $\bar{T}_e=\bar{T}_i$~20keV(±0.7keV), E_b=600keV. The figures show the driven current I_P, the average electron density $\bar{n}_e$, the toroidal field B_{to} at $R=R_o$ and the energy gain Q. The beam power is known as P_f/Q. Throughout these calculations, Z_{eff} was kept to be 2.2 with 5% Helium concentration in the fuel ions and 0.04% Xe impurity, which was added for Z_{eff} control. The D/T ratio was 50/50. If any lower Z impurities are to be considered instead of Xe, the fusion output and the Q value would reduce slightly. In the B_{to} plots, the B_{to} maximum limits are also shown. When the B_{to} is higher than the limit line, the maximum field on the toroidal field coils, B_{max}, will exceed one of the present technological limit; B_{max}=12T. The value B_{max} was defined as

$$B_{max} = B_{to}R_o/(R_{min}-D_s) , \qquad (18)$$

where D_s is the shield thickness between the toroidal field coils and the first wall. Through the present DEMO machine study, D_s=0.8m was assumed for any plasma size. Therefore, a B_{to} limit is lower for a smaller machine, and the bean type, which has an indentation, results in a lower limit, compared with the D-type.

The findings from Fig.7 are as follows: The bean type requires a lower B_{to} and smaller I_P to obtain the same fusion output, in comparison with the D-type. This fact becomes clearer when we compare the bean and D-machines with the same R_o*, i.e. with nearly the same plasma volume. Cases where R_o*=3.86m and 4.55m are indicated by solid circles and crosses, respectively. In both cases, the average electron density $\bar{n}_e$ is nearly the same for the same P_f value. However, the currents to be driven in the bean type machines are less than those in the D-type. Therefore the driver power for the bean is lower and the Q value is larger than of the D-type. For DEMO-3, P_b=106MW and Q~4.5 for the D-type at P_f=500MW, while Q~6 is possible with P_b=83MW for the bean. The beam power can be

reduced by about 30% in the bean shaped tokamaks. A further important feature is that the Q value seems to saturate in a large P_f region for the D-type in contrast with the bean.

In the bean cases, sufficient margins remained in B_{t0} against the B_{max} limit for the 500 MW class machines. On the other hand, the toroidal field strength is nearly critical for the D-type.

the results in Fig.7 show that the Q value strongly depends on the fusion output P_f, but is nearly independent from the machine size. Once the output power is chosen, the Q value is also determined inescapably. The most compact bean case, where R_0*=3.18m, seems to result in a slightly smaller Q. As a small machine requires a higher density for the same fusion output, most of the beam power for each beamlet tends to deposit on the edge region. This fact reduces ξ_b in Eq.(2). Therefore, the current drive efficiency would be deteriorated. Moreover, a smaller ξ_b (larger pitch angle) brings about some drive current loss, due to the trapped ion orbits. As a result of the efficiency deterioration, the Q value for a small machine would be reduced. This Q reduction may be recovered by beam energy optimization. The present 600keV beam is optimized for the R_0*=3.86m machines, as described later.

The ratio of beam beta to total beta, β_b/β_t, is plotted in Fig.8. The portion of the beam pressure in the total pressure is larger for a lower output and/or a more compact machine. As a large beam pressure leads to a fuel pressure drop, a low output and a too compact size would be undesirable. The reason for the β_b/β_t increment in a compact machine is interpreted by the current drive efficiency deterioration, due to the large beam ion pitch angle, as described above.

The energy confinement time τ_E, required to sustain the above beam driven equilibria, can be evaluated by the following power balance equation;

$$\frac{3}{2}(\bar{n}_e\bar{T}_e+\bar{n}_i\bar{T}_i)V_P/\tau_E = \frac{1}{5}P_f+(1-f_s)P_b \ , \qquad (19)$$

where the first term on the right hand side means alpha heating and the

second term is the beam heating power. The τ_E values determined by Eq.(19) are plotted in Fig.9, where the equilibria for DEMO-2 and 3 (D and bean), shown in Fig.7, are compared. The energy confinement times τ_{K-G}, estimated by Kay-Goldston type scaling [27], are also plotted in the figure for reference:

$$1/\tau^2_{K-G} = 1/\tau^2_{OH} + 1/(k\cdot\tau_{AUX})^2, \quad \begin{cases} k=1 \text{ for L-mode} \\ k=2 \text{ for H-mode} \end{cases} \tag{20}$$

The required τ_E has fallen within the middle range, between the L-mode and H-mode confinements, except for one of the R_0*=4.55m D-type cases. When considering the over 500 MW DEMO machines, the L-mode confinement seems to be nearly sufficient to sustain the beam driven equilibria, except for the R_0*=4.55m D-type cases.

5.3 $\bar{T}_e$ and $\bar{T}_i$ Scan

In the previous section, it was assumed that the electron temperature $\bar{T}_e$ was equal to the ion temperature $\bar{T}_i$. In the steady state burning phase, most portions of the alpha particle heating power (90% at T_e=20keV) go to the background electrons. Therefore the electron temperature is usually higher than the ion temperature or nearly same each other in inductively driven tokamaks. In the case of r.f.driven reactors, $\bar{T}_e \gtrsim \bar{T}_i$ is expected, because most of the r.f.current drive power is absorbed by electrons. On the other hand, in the beam driven reactor, the injected fast ion divides its initial energy among the background electrons and ions as it thermalizes. For the 600keV beam injection into the $\bar{T}_e$=20keV plasma, the ratio between the energy going to the electrons and ions is about 50/50[3]. Therefore a $\bar{T}_i$ higher than $\bar{T}_e$ can be expected in the beam driven reactors. Of course, these temperatures depend on ion and electron thermal diffusivities. Unfortunately, it seems that there is no reliable model for these transport phenomena to date, especially for electron thermal diffusivity. In this study, therefore, the authors regarded $\bar{T}_e$ and the ratio $\bar{T}_e/\bar{T}_i$ as scan parameters, instead of evaluating these values under an ambiguous transport model assumption.

The results from $\bar{T}_e$ and $\bar{T}_e/\bar{T}_i$ scanning are summarized in Fig.10. The Q value and the toroidal field strength, required to gain 330 MW fusion output, are shown as functions of $\bar{T}_i$, where the DEMO-2 bean (R_0*=3.86m) are used and the beam energy is 600keV again. The solid line represents the $\bar{T}_e$=$\bar{T}_i$ case. the broken line represents the $\bar{T}_e \neq \bar{T}_i$ case where $\bar{T}_e$ is kept at 20keV.

For the $\bar{T}_e$=$\bar{T}_i$ cases, increasing $\bar{T}_e$ results in a current drive efficiency improvement. However, if the B_{t0} is kept constant, the fusion power is reduced with the $\bar{T}_e$(=$\bar{T}_i$) increment, because the total beta are restricted. In order to maintain the 330MW output, the B_{t0} value must be increased with $\bar{T}_e$(=$\bar{T}_i$). Increasing $\bar{T}_e$(=$\bar{T}_i$), up to 25keV from 20keV, required 9% B_{t0} increment, while the Q value was also improved by 11%. On the other hand, to increase $\bar{T}_i$ up to 25keV, from 20keV, while keeping $\bar{T}_e$=20keV, made the same 11% Q enhancement possible

with a negligible B_{t0} increment(~1%). Therefore, the $\bar{T}_i > \bar{T}_e$ operation is obiously attractive for steady state tokamaks. The high $\bar{T}_i$ feature of a beam driven reactor could bring about some improvement in the Q value.

The plasma pressure composition and the beam power distribution P_{INJ} are compared in Fig.11, where the plasma is for DEMO-2 bean (R_0*=3.86m), E_b=600keV and $\bar{T}_e=\bar{T}_i$, again. The $\bar{T}_e$ values were scanned from 15keV to 25keV but the fusion output P_f was maintained at 330MW (±10MW) by B_{t0} adjustment. The fast alpha pressure becomes pronounced with increasing $\bar{T}_e$. This is a natural feature which had been predicted by a simple Fokker-Planck calcuration[26]. This feature is undesirable, because the alpha pressure component increment causes a fuel component drop. Since the current drive efficiency, however, improves with a higher $\bar{T}_e$, the Q value still improves with $\bar{T}_e$. On the other hand, there is no pronounced change in the beam pressure profile and in the required beam power distribution P_{INJ}, while the total injection power changes.

5.4 Temperature Profile Scan

The density profile is determined automatically in the reverse solution so as to satisfy the critical beta pressure profile, once a temperature profile has been given. A different choice of temperature profile leads to another solution with a different density profile. It is usually believed that the Q-value and the fusion power strongly depend on the density and temperature profiles. It is true, when the pressure profile is not maintained in the same form. The fusion output would change by a factor up to about 2 for various temperature and density profile combinations. The results of temperature profile scan are summarized in Fig.12, where the temperature profiles are scanned from a parabolic profile [$\propto 1-(r/a)^2$] to a very broad profile [$\propto 1-(r/a)^{10}$] for DEMO-3 D-type (R_0*=4.55m) using $\bar{T}_e=\bar{T}_i$=20keV, B_{t0}=4.3T and E_b=600keV. Contrary to the above expectation, the changes in Q, P_f and I/P_{abs} are comparably small (less than 20%) throuth this temperature scan. This is because a peaked temperaure profile results in a broad density profile and vice versa in order to maintain the marginal stable pressure profile. This is a special feature of the reverse solution, and possibly it is more realistic, because the peaked density with the peaked temperature, namely the very peaked pressure profiles are usually unsuitable for any high beta plasma equilibrium in the first stability regime.

The beam shinethrougth f_s is minimized at α_j=10, and at the same time, the fusion power and the Q value are maximized with a small I/P_{abs} value degradation. Therefore, the broad temperature profile were chosen throuth the other parameter scans, in order to obtain the optimum reactor performance.

The injection power distribution $P_{inj}(z)$ and the density profiles are also shown in Fig.12 with the temperature profiles used in the computations. Although the Q, P_f and I/P_{abs} value changes have been small, the P_{inj} form is greatly modified by the temperature profile choice. Since the broad temperature profile leads to a high $\bar{T}_e/\bar{n}_e$ ratio (therefore a high j/p_e value) near the plasma edge, the broad current profile, required for the critical beta equiribrium, can be driven by the centrally peaked beam power distribution. Pellet injection

fuelling would be suitable to generate such parabolic density and broad temperature profiles.

5.5 Beam Energy Scan

Results of beam energy scan for DEMO-2 bean type (R_0*=3.86m) and DEMO-3 D-type (R_0*=4.55m) are shown in Fig.13 and Fig.14, where $\bar{T}_e=\bar{T}_i$=20keV and E_b was scanned from 400keV to 1.0MeV. When beam shinethrough is not considered, the simple Fokker-Planck calculation gives 1.5~2.0 MeV as the optimum beam energy for current drive in $\bar{T}_e$=20keV plasma. In the previous beam current drive analysis by the DRIVER code [5], where shinethrough was taken into account but a parabolic current profile was assumed without any MHD equilibrium/stability calculations, it was also concluded that the optimum beam energy was about 1.0 MeV. However, the present results, where strictly consistent current and pressure profiles are used, differs much from those previous calculations. The Q value saturates at E_b~600keV for both bean and D-types. One of the obvious reasons for this saturation is the beam shinethrouth increment, which is pronounced for E_b over 600keV. The profile of $P_{INJ}(Z)$ is shown at the bottom of each figure. When E_b increases, more power should be injected in the edge region. This is because each beamlet penetration becomes deep, with E_b increment, and the edge injection power should be increased, in order to maintain the edge current profile. Since this edge injection power increment furthers the beam shinethrough from the plasma edge, the shinethrough fraction f_s increases rapidly with the E_b increase.

There is a second reason for the Q saturation, namely, the reduction in TCT power, P_{TCT}. As shown in Figs.13 and 14, P_{TCT} component in the total output accounts for 10~20% in the bean type and for 12~28% in the D-type. The TCT gain P_{TCT}/P_b takes its maximum at E_b=170~250keV and decreases for a higher E_b[26]. Therefore, the E_b increment results in fusion power reduction and tends to promote the Q saturation.

Since P_{TCT}/P_b is of the order of unity for $E_b>500$keV[5], the TCT effect

changes the Q value within unity, even in the maximum case. This effect would be negligible for a large Q (>>10) reactor. However, for the DEMO machines with Q~5, it is comparatively important.

The present E_b scan shows that the optimum beam energy for the DEMO machine is about 600keV and that a higher beam energy would enhance beam shinethrough from the low density edge.

The above E_b scan was made with the broad temperature profile, as described in Section 4. The aditional E_b scan was also made with a parabolic temperature profile. But the tendency of the Q-saturation for the over 600~800 keV beams did not change.

The beam shinetrough and the beam deposition profile would be changed, if a the beam stopping cross-section is enhanced by a multi-step ionization (MSI) process [32]. However, our calculation, including approximetely the MSI cross-section enhancement, clarified that this effect does not change the above Q-saturation, because this Q-saturation still occurs by the TCT power reduction.

6. PARAMETER SCAN FOR POWER REACTORS

The parameters required to sustain power reactor grade tokamaks have been scanned for the machine sizes in Table 1 (POWER 1-6), as well as for the DEMO machine. The several giga-watts thermal output power reactors are considered here. The main interest in this section is the possibility of sufficiently high Q operation to use it as a commercial power reactor. An over 30 Q value would be desirable, if possible, and at least Q~20 would be required to obtain a reasonable electric output gain. When assuming 33% thermal-electric conversion efficiency and 50% overall efficiency for the current driver, increasing Q from 10 to 20 results in a 75% increment in electric output, while the case from 20 to 30 enhances electric output by only 14%.

The Q values, obtained from the power reactor scan, are plotted in Figs.15 and 16 as functions of P_f, where 3 sizes for both bean and D-types(Table 1) with $\bar{T}_e(=\bar{T}_i)$=20,25,30keV, and E_b=1.5 and 2.0MeV were investigated. Here, Z_{eff}=2.0 (5% He and Xe impurity) was assumed. The magnetic field strength B_{t0}, to gain the required output power, is also plotted in the figures. However, only the cases where E_b=1.5MeV, $\bar{T}_e$=20keV and 30keV are shown in these B_{t0} plots to simplify the figures. However the B_{t0} value in the E_b=2.0MeV cases are nearly identical to those in the 1.5MeV cases. The B_{max} values have been calculated with D_s=1.0m in this power reactor scan.

As shown in the figures, once the plasma temperature has been given, the Q values are nearly determined as a function of P_f for both bean and D-types. This feature is similar to the DEMO cases. However, in the present cases, a tendency toward Q saturation is found in the bean case as well as in the D-type cases. The values for Q, however, are larger by about 30% in the bean cases, in comparison with the D-type cases.

The Q value can be enhanced by the high temperature operation up to 30keV. With the bean shaped plasma, Q=20 is achievable with P_f~4.5GW and $\bar{T}_e$=30keV, while some head margin against the B_{max} limit still remains, except for the smallest R_0*=4.09m case. On the other hand, the Q value for the D-type machine

does not exceed sixteen. In order to operate the D-type reactor with a Q value around 16 with $\bar{T}_e$=30keV, the R_0^*=6.5m machine is not suitable, due to the B_{max}=12T limit. Even if B_{max} over 12T is available, it seems that Q over 20 is not achievable because of the Q saturation in the large P_f region.

The Q value change by E_b seems to be negligible in $1.5 \lesssim E_b/(MeV) \lesssim 2.0$ range. This would result from the cancellation between the current drive efficiency improvement and the shinethrough increment.

The f_s values are summarized in Fig.17. The shinethrough was localized near the edge, and the shinethrough through the plasma center was negligible. Under the same output operation, f_s increases for a larger machine. Since the line density along the beam line and the fusion power P_f are proportional to $\bar{n} R_0$ and $\bar{n}^2 R_0^3$ respectively, the line density decreases with the R_0 increment, when P_f is kept constant. Therefore the above feature, on f_s, is reasonable.

The D-type reactor size should be inescapably large ($R_0^* \geqq 7.0$m) due to the B_{max}=12T limit, as described above. On the other hand, the bean shaping makes a smaller machine size possible. However the minimum machine size would be restricted by neutron wall loading P_N. The value P_N for the present bean type reactor is roughly expressed by

$$P_N \sim 5 \left(\frac{P_f}{4.5GW}\right)\left(\frac{4.55m}{R_0^*}\right)^2 \quad [MW/m^2] \ , \tag{21}$$

where a rectangular cross-section first wall with $2.4\kappa a$ in height and 2.4a in width are assumed. In a reference case (R_0^*=4.55m, P_f=4.5GW), P_N attains 5MW/m². which would be a very severe condition for the first wall. When POWER-3 (R_0^*=5m) is chosen, P_N is reduced down to 4 MW/m². However, the shinethrough would be doubled as shown in Fig.16. Lowering P_f reduces the wall load, but it decreases the Q value and enhances shinethrough.

When choosing the compact high beta machine, large wall loading would be a critical issue in any case. If P_N=5MW/m² is acceptable, the advisable

size for the bean type plasma is R_o^*=4.55~5.0m.

Finally, the problem in regard to the power balance in the reactor grade plasma remains. An over-ignited reactor, like the present cases, should have its confinement controlled by some burn control technique. Many methods for burn control have been proposed to date. However, such problem is beyond the scope of this study, so the over ignited reactor confinement is not discussed here.

7. DISCUSSION

Although beam shinethrough in the D-type machine is somewhat smaller than the bean case, 5%~10% shinethrough is inevitable in most of the cases. The impact by such shinethrough could not be disregarded in the first wall or the beam damper design, because the beams are operated in steady state. As shown in Section 6, increasing the machine size brings about a larger shinethrough, and the smaller bean type machine would be restricted by the neutron wall loading, while the D-type machine size would be restricted by the B_{max} limit, rather than the wall loading. Ultimately, the beam shinethrough would set a severe limitation for compact high beta bean tokamaks sustained by the beam driver.

Most of the shinethrough is generated by the beam passing the plasma edge. If this shinethrough from the edge can be suppressed, overall shinethrough will reduce considerably. Such shinethrough reduction may be possible by a combination of the beam current driver with an LHRF current driver. The weakness of LHCD is the difficulty driving the current in high density plasmas. However, it could drive some currents in the low density edge region. The edge current driven by LHCD can be controlled very flexibly by 'non-uniform phasing' in the LHRF grill launcher[30,31]. A modification of the present reverse solution code to combine with the LHCD calculation is now being planned.

Boley et al. pointed out the possibility of enhancement in the neutral beam stopping cross-section due to multistep collision processes [32]. Although some further experimental verifications on their theoretical prediction are necessary, their calculation has shown that a stopping cross-section enhancement could be expected by a 1.5~2.0 factor for the beam energy used for the current drive.

Our code was modified to investigate the MSI cross-section enhancement effect. The enhancement rate $1+\delta$ was approximetely given by a fitting function, which was folmulated using the result in Ref.[33]. The model includes the

δ-dependence on E_b and n_e. Using this modified version, the E_b scan for D-type plasma (Section 5.5 and Fig.14) was recalculated. It was found that the shinethrough was reduced by the MSI effect. For example, 11% shinethrough (the E_b=1.0MeV case in Fig.14) decreased to 7% , when the MSI effect was assumed. However, this shinethrough reduction rate is much smaller than the estimation by a uniform plasma calculation in Ref.[33]. This is because, most of the shinethrough occurs on the beamlets passing the low density edge region, and the MSI cross-section enhancement for these beamlets is small. [Note that the MSI enhancement rate strongly depends on the density. For the low density ($\lesssim 10^{19}m^{-3}$), $1+\delta$ is almost unity.]

The beam power profile $P_{inj}(z)$, to sustain the critical beta equilibrium, was greatly changed by the MSI, because the MSI enhancement is pronounced in the plasma central region. However, the changes in the Q and I/P values were negligible, as desdribed in Section 5.5.

The existence of the MSI cross-section enhancement is one of the critical issues for the beam driven reactor, because the impact in beam driver design by the MSI effect will not be small. Further theoretical and experimental study is required to verify this effect.

8. SUMMARY AND CONCLUSION

It has been shown that the bean type (β=20.9%) and the D-type (β=6.05%) critical beta equilibria can be sustained in steady state by beam driven currents only. The optimum energies, for DEMO size machines with several hunded MW thermal output and for power reactors with several GW thermal output, are about 600keV and 1.5MeV, respectively.

The parameter scans for various size tokamaks showed that, once the plasma shape and the plasma temperature are given, the achievable energy gain Q is inescapably dependent on the fusion output power value, but is rather independent from the machine size. Namely, the tokamak size increment brings about no inprovement in the Q value, if the fusion power does not change. The Q value for bean type is always 20~30% larger than the Q value for the D-type. With bean shaped reactors, the Q value over 20 can be achieved with R_0~5m and B_{t0}~4 Tesla, where the maximum magnetic field B_{max} on the toroidal coils is much less than 12 Tesla. On the other hand, achieving the Q value over 16 seems to be difficult with the conventional D-type tokamak reactors, and the B_{max}=12 Tesla limit becomes critical. The beam power required to drive the currents is also smaller in the bean cases, under the same output power operations.

When the thermal output is kept constant, increasing the plasma size results in a beam shinethrough increment. For the bean type reactor, a smaller size reduces the shinethrough, but the minimum size would be restricted by the neutron wall loading. The advisable size, for bean with P_f=4.5GW, is R_0~5m, where a Q value around 20 can be obtained. On the other hand, in the D-type case, Q and P_f are restricted up to 16 and 3.5GW even when a 7.5m size machine is assumed.

The present study shows a new merit of the bean type machine in addition to its high beta feature, namely, the possibility of a higher Q operation with a lower current driver power. Although the bean type tokamak has some severe engineering demerits, for example the inside pusher coils, its

application in a future steady state tokamak should be seriously considered. A very high current machine with D-type high beta plasma is not advisable for use in steady state operation, because it will require over 100MW driver power, even for the DEMO size machine.

ACKNOWLEDGEMENTS

The authors gratefully thank Drs. K. Shinya, T. Amano and Y. Hamada for their interest and valuable comments throughout this study. This work was carried out on the computer at the Institute of Plasma Physics of Nagoya University under its collaborative research programme.

REFERENCES

[1] TROYON, F., GRUBER, R., SAURENMANN, H., SEMENZATO, S. and SUCCI, S., Plasma Phys. Control. Fusion 26(1984)209.

[2] YAMAZAKI, K., AMANO, T., NAITAU, H., HAMADA, Y. and AZUMI, M., Nucl. Fusion 25(1985)1543.

[3] MIKKELSEN, D.R. and SINGER, C.E., Nucl. Technol/Fusion 4(1983)237.

[4] OHKAWA, T., Nucl. Fusion 10(1970)185.

[5] OKANO, K., YAMAMOTO, S., SUGIHARA, M. and FUJISAWA, N., Japan Atomic Energy Research Institute Report, JAERI-M 87-209, (1988).

[6] AXON, K.B., et al., Proc. 9th IAEA Int. Conf. on Plasma Phys. and Control. Fusion Research, Vol.1, (1981)413.

[7] OKANO, K., YAMAMOTO, S. and SUGIHARA, M., in INTOR Related Specialists' Meeting on Non-Inductive Current Drive, Garching, (1986), published in Japan Atomic Research Institute Report, JAERI-M 87-106, 1987.

[8] EHST, D.A., Nucl. Fusion 25(1985)629.

[9] EHST, D.A., EVANS, K. Jr. and IGNAT, D.W., Nucl. Fusion 26(1986)461.

[10] YAMAMOTO, S., OKANO, K., et al., in Proc. 11th IAEA Int. Conf. on Plasma Phys., and Control. Fusion Research, Vol.3, (1987)267.

[11] OKANO, K., SHINYA, K. and YAMATO, H., in 'Fusion Reactor Critical Issues', IAEA-TECDOC-441, IAEA, Vienna, (1987)49.

[12] SYKES, A., TURNER, M.F. and PATEL, S., in Proc. 11th Eropean Conf. on Control. Fusion and Plasma Phys., Aachen, Vol.2, (1983)363.

[13] GRUBER, R., et al., Comput. Phys. Commun., 21(1981)323.

[14] GRUBER, R., et al., Comput. Phys. Commun., 24(1981)363.

[15] NAITOU, H. and K. YAMAZAKI, IPPJ-837, Institute of Plasma Physics, Nagoya, Japan (1987), accepted for publication in Nucl. Fusion.

[16] CALLEN, J.D. and DORY, R.A., Phys. Fluids, 15(1972)1523.

[17] CONNOR, J.W., HASTIE, R.J. and TAYLOR, J.B., Phys. Rev. Lett., 40(1978)396.

[18] GAFFEY, J.D., J. Plasma Phys., 16(1976)149.

[19] OKANO, K., Plasma Phys. Control. Fusion, 29(1987)1115.

[20] START, D.F.H. and CORDEY, J.G., Phys. Fluids, 23(1980)1477.

[21] EHST, D.A., et al., Argonne National Laboratory Report, ANL/FPP/TM-213, (1987).

[22] OKANO, K., et al., Tokamak Concept Innovations. IAEA-TECDOC-373, IAEA, Vienna (1986)209.

[23] OHARA, Y., et al., ibid, (1986)305.

[24] SHINYA, K., private communication.

[25] For example, NAITOU, H., et al. Nucl. Fusion, 27(1987)765.

[26] JASSBY, D.L., Nucl. Fusion 17(1977)309.

[27] GOLDSTON, R., Plasma Phys. Control. Fusion, 26(1984)87. And, KAYE, S.M., Phys. Fluids 28(1985)2327.

[28] CHALLIS, C., et al., in Proc. 14th European Conf. on Control. Fusion and Plasma Phys., Madrid, (1987)1026.

[29] ZARNSTRORFF, M.C., et al., ibid, (1987)144.

[30] HATAYAMA, A., SUGIHARA, M., OKANO, K., SAITO, Y., TACHIKAWA, N. and FER Plasma Design Group., ibid, (1987)1046.

[31] OKANO, K., HATAYAMA, A., and SUGIHARA, M., 'Lower Hybrid Wave Spectra Broadening and Current Profile Control by Non-Uniform Phasing of Grill Launchers', to be published.

[32] BOLEY, C.D., JANEV, R.K. and POST, D.E., Phys. Rev. Lett. 52(1984)534.

[33] DEVOTO, R.S., et al., in U.S. contribution to ITER Workshop, Garching, March 1988.

[34] HAMADA, Y., KITAGAWA, S., MATSUOKA, K., MATSUURA, K., OGAWA, Y., et al., in Proc. of 10th IAEA Int. Conf. on Plasma Phys. and Control. Nucl. Fusion Reseach, IAEA, Vienna, Vol.3, (1985)353. And, MIYAHARA, A., HAMADA, Y., OGAWA, Y., MATSUOKA, K., KITAGAWA, S., et al., Nucl. Engineering and Design/Fusion 4(1987)269.

[35] OKANO, K. et al., in U.S.-Japan Workshop on Non-Circular Tokamaks, San Diego, 19-23 Jan. 1986.

CAPTIONS

Table 1. Machine sizes and equilibrium parameters used in parameter scans.

Table 2. Beam line parameters.

Fig.1 Schematic drawing of beam line and its power distribution $P_{INJ}(z)$.

Fig.2 Critical beta equilbria of the D- and bean types, where β_t=20.9% for the bean type and β_t=6.05% for the D-type.

Fig.3 Definition of plasma shape parameters. In case of D-type, d=0 and $R_0^*=R_0$.

Fig.4 Example of density profile in converged solution, where R_0^*=3.18m (bean type), $\bar{T}_e=\bar{T}_i$=20.7keV and B_t=2.7T. The temperature profile is also shown.

Fig.5 Example of beam generated critical beta equilibria (bean type), where R_0^*=3.86m, $\bar{T}_e=\bar{T}_i$=20keV. The fusion power P_f=647MW with B_t=2.5T.

Fig.6 Example of beam generated critical beta equilibria (D-type), where R_0^*=4.55m, $\bar{T}_e=\bar{T}_i$=20keV. The fusion power P_f=631MW with B_t=4.5T.

Fig.7 Energy gain Q and other parameters, as functions of the fusion output, where E_b=600keV, $\bar{T}_e=\bar{T}_i$=20keV.

Fig.8 Beam pressure components in total pressures.

Fig.9 Energy confinement time τ_E for beam generated equilibria, where τ_E is compared with Kaye-Goldston scaling.

Fig.10 Q-enhancement by temperature increment.
Solid lines represent the $\bar{T}_e=\bar{T}_i$ case.
Broken lines show the $\bar{T}_i \neq \bar{T}_e$ case with $\bar{T}_e$=20keV.

Fig.11 Change in pressure components by $\bar{T}_e$ variation, where R_0^*=3.86m (bean), E_b=600keV. P_f was maintained at 330MW(±10MW).

Fig.12 Result from T_e-profile scan, where R_0^*=4.55m D-type. B_{t0}=4.3T, $\bar{T}_e=\bar{T}_i$=20keV.

Fig.13 Result from beam energy scan for R_0^*=3.86m bean type tokamak. B_{t0}=2.4T and $\bar{T}_e=\bar{T}_i$=20keV.

Fig.14 Result from beam energy scan for R_0^*=4.55m D-type tokamak. B_{t0}=4.3T and $\bar{T}_e=\bar{T}_i$=20keV.

Fig.15 Summary plots for bean type power reactor scans.

Fig.16 Summary plots for D-type power reactor scans.

Fig.17 Shinethrough fraction f_s as a function of P_f, where $\bar{T}_e=\bar{T}_i$=25keV and E_b=1.5MeV. (a) bean type case. (b) D-type case.

		Bean type			Dee type		
	R_0^*	R_0	a	V_P	R_0	a	V_P
DEMO 1	3.18	3.50	0.82	140	—	—	—
2	3.86	4.25	1.00	246	3.86	1.41	266
3	4.55	5.00	1.18	404	4.55	1.66	436
4	5.20	—	—	—	5.20	1.90	568
POWER 1	4.09	4.50	1.06	276	—	—	—
2	4.55	5.00	1.18	404	—	—	—
3	5.00	5.50	1.30	488	—	—	—
4	6.50	—	—	—	6.50	2.38	888
5	7.00	—	—	—	7.00	2.56	1030
6	7.50	—	—	—	7.50	2.74	1182
Aspect ratio A		$2.75[R_o/(R_{max}-R_{min})]$			2.75		
Plasma elongation κ		3.32			1.80		
Plasma triangularity δ		1.50 [indent.=0.29]			0.30		
Toroidal beta $\bar{\beta}_t$		20.9%			6.05 %		
Poloidal beta $\bar{\beta}_p$		0.699			0.486		
Plasma current I_P		$I_P = 1.24\, R_o B_{to}$ (MA)			$I_P = 0.915 R_o B_{to}$ (MA)		
q_ψ on surface		3.22			2.05		
q_ψ at center		1.09			1.15		

Table 1

Beam Line Parameters

	for Bean		for Dee
Beam No.	1	2	1
w (beam with) / R_0	0.10	←	0.11
h (beam height) / R_0	0.80	0.27	1.21
R_{tang} (orientation) / R_0	0.90	0.80	0.89
Z_h (vertical shift) / R_0	0	±0.535	0
θ_v (vertical angle)	0	←	0
Power profile mesh (height x width)	15x3	10x2	25x3

Table 2

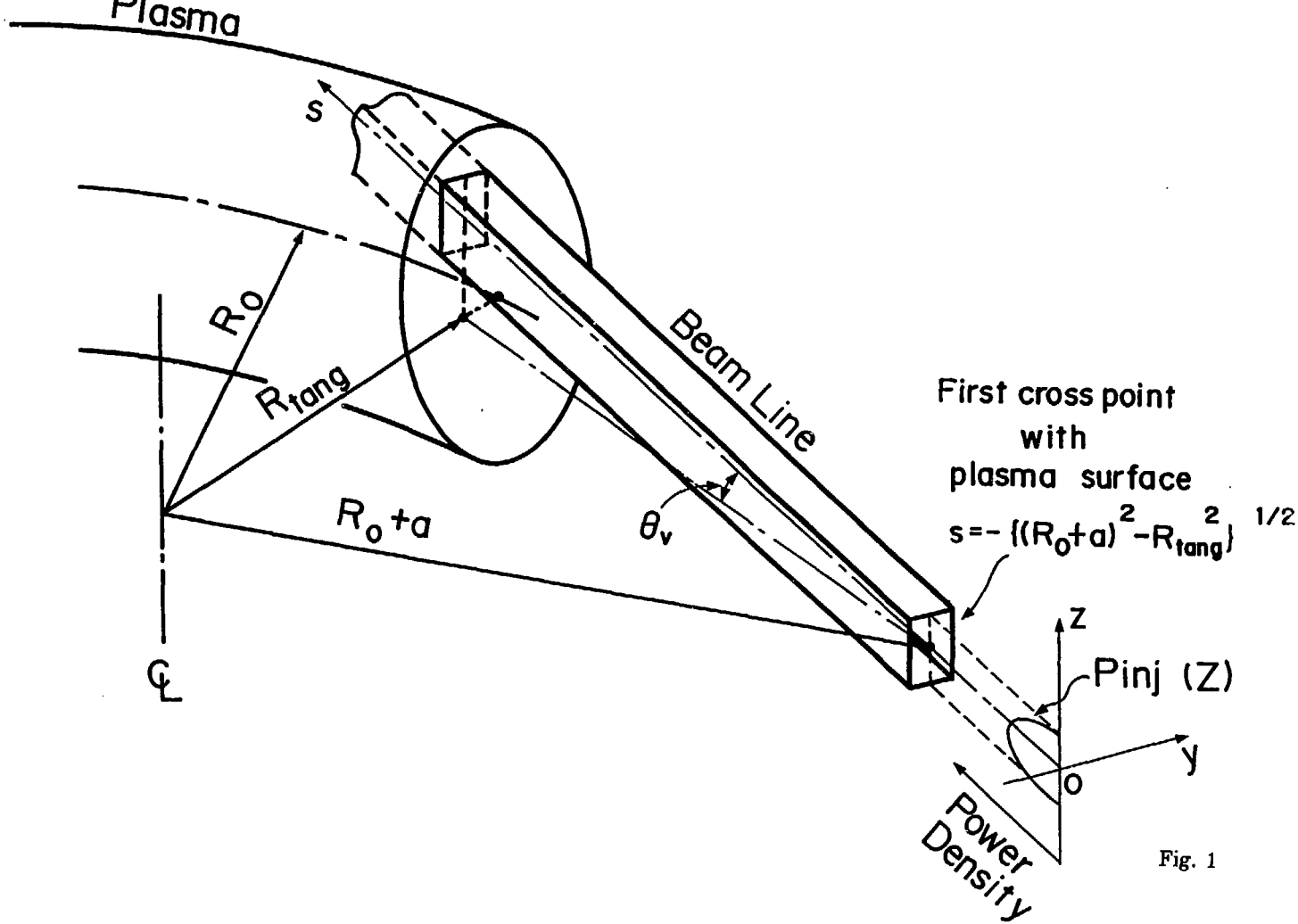
Plasma
s
R_o
R_{tang}
Beam Line
R_o+a
θ_v
First cross point
with
plasma surface
$s=-\{(R_o+a)^2-R_{tang}^2\}^{1/2}$
z
Pinj (Z)
y
o
Power
Density

Fig. 1

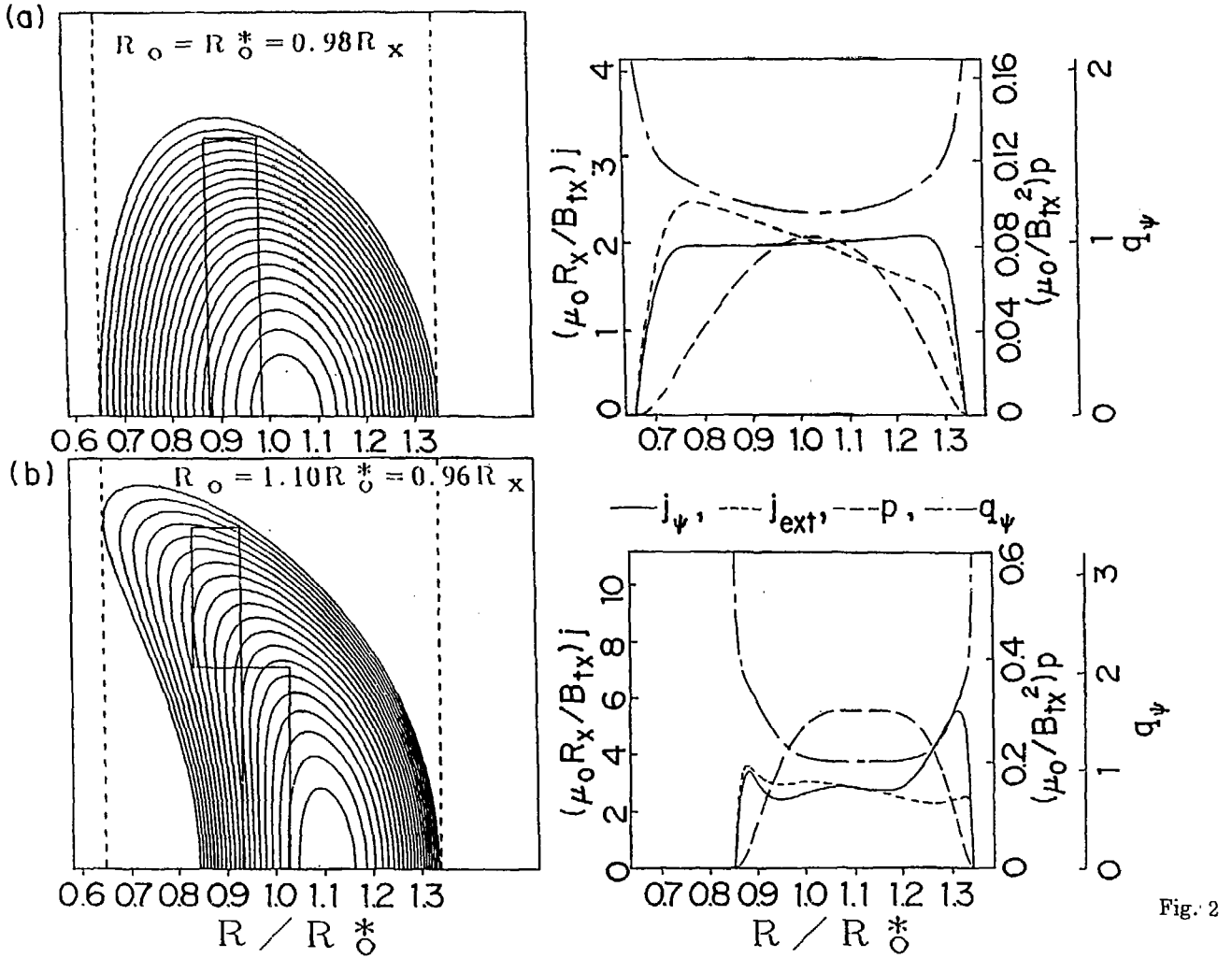
(a)
$R_o = R^*_o = 0.98 R_x$
(b)
$R_o = 1.10 R^*_o = 0.96 R_x$
0.6 0.7 0.8 0.9 1.0 1.1 1.2 1.3
R / R*o
$(\mu_o R_x/B_{tx})j$
$(\mu_o/B_{tx}^2)p$
q_ψ
j_ψ, j_{ext}, p, q_ψ

Fig. 2

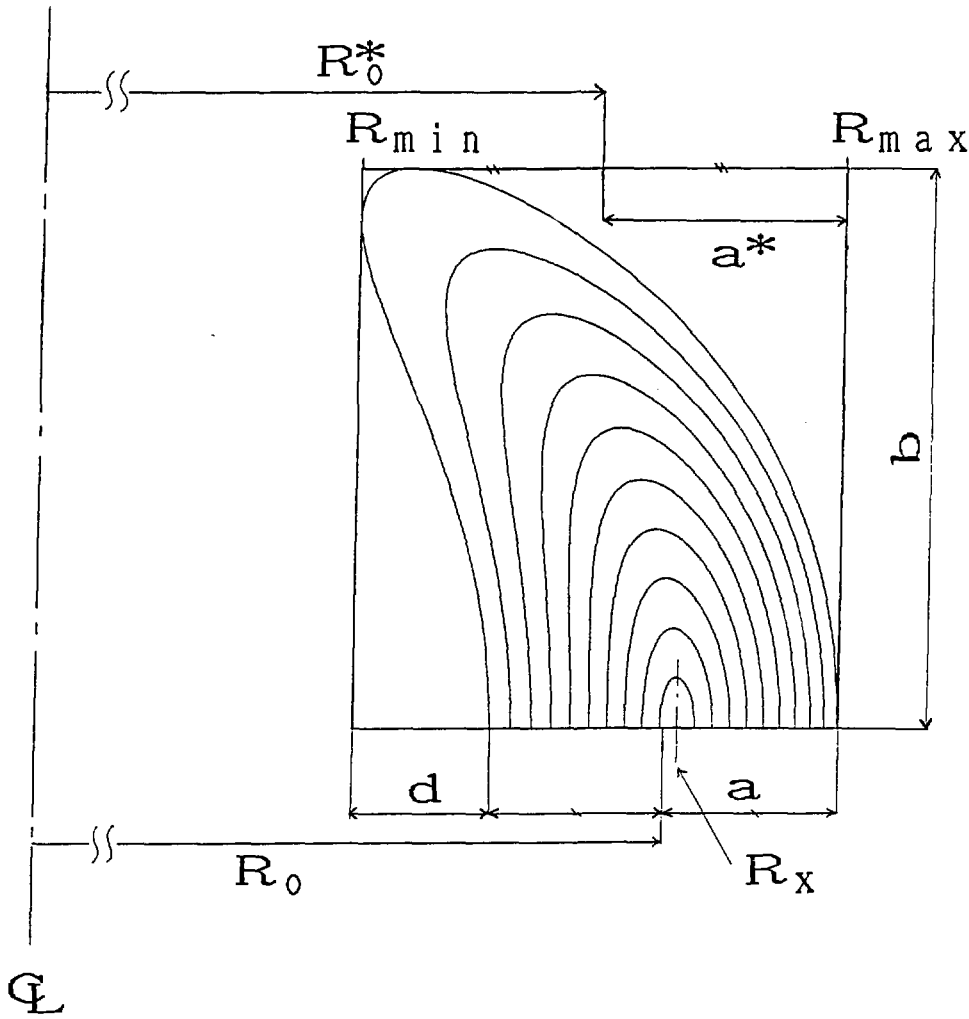

Fig. 3

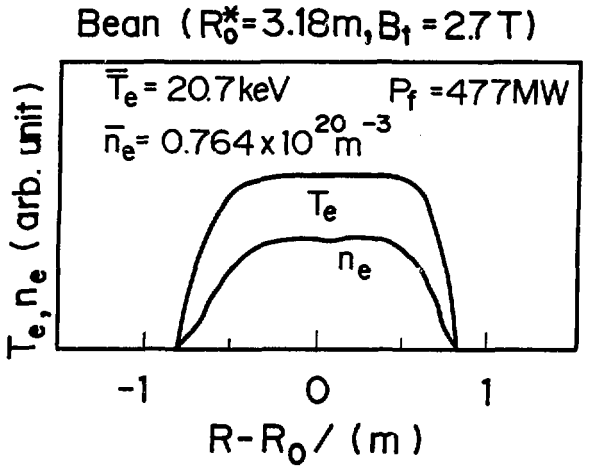
Bean (R_0^*=3.18m, B_t = 2.7 T)
$\bar{T}_e$ = 20.7 keV
P_f = 477 MW
$\bar{n}_e$ = 0.764 x 10^{20} m^{-3}
T_e
n_e
T_e, n_e (arb. unit)
-1
0
1
R-R_0 / (m)

Fig. 4

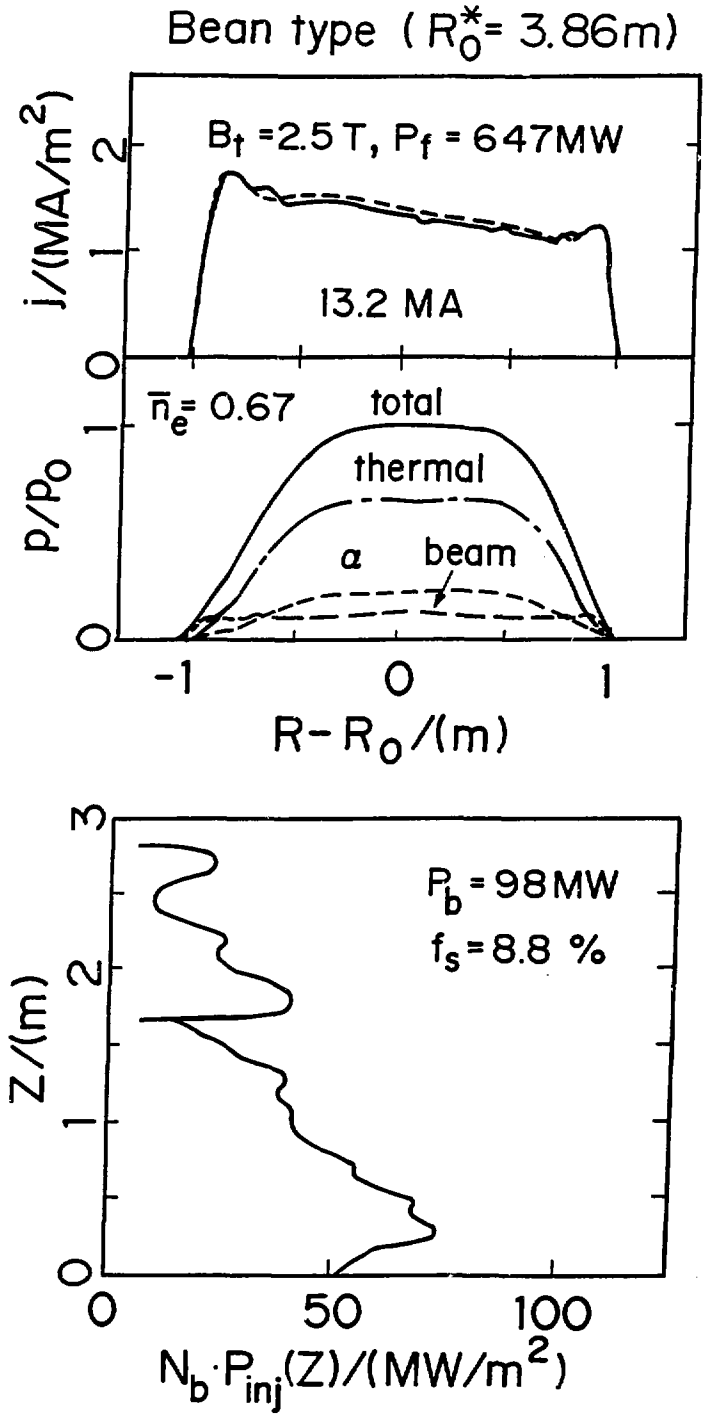
Bean type (R_0^*= 3.86m)
B_t =2.5 T, P_f = 647MW
13.2 MA
j/(MA/m^2)
$\bar{n}_e$= 0.67
total
thermal
α
beam
P/P_0
R−R_0/(m)
P_b = 98MW
f_s = 8.8 %
Z/(m)
$N_b \cdot P_{inj}(Z)$/(MW/m^2)

Fig. 5

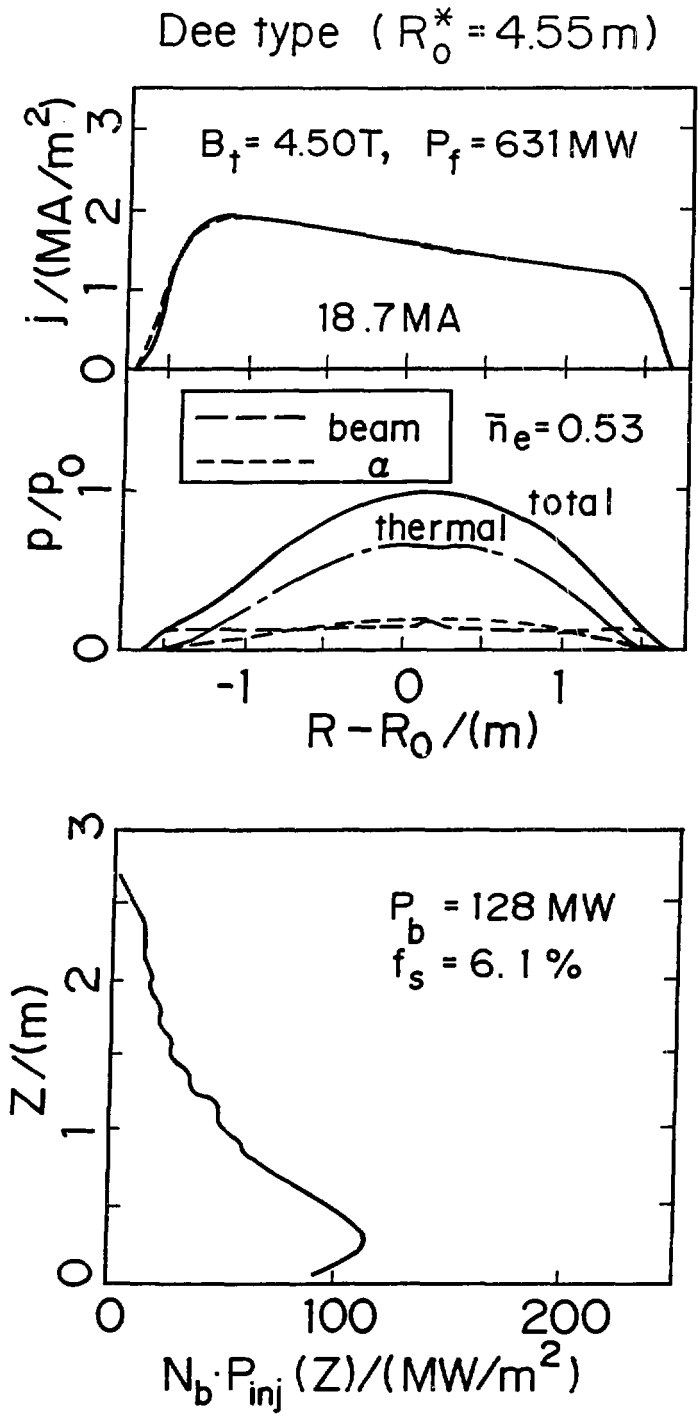
Dee type ($R_0^* = 4.55$ m)
$B_t = 4.50$T, $P_f = 631$MW
18.7MA
$j/(MA/m^2)$
beam
α
$\bar{n}_e = 0.53$
total
thermal
p/p_0
$R - R_0/(m)$
$P_b = 128$ MW
$f_s = 6.1$ %
$Z/(m)$
$N_b \cdot P_{inj}(Z)/(MW/m^2)$

Fig. 6

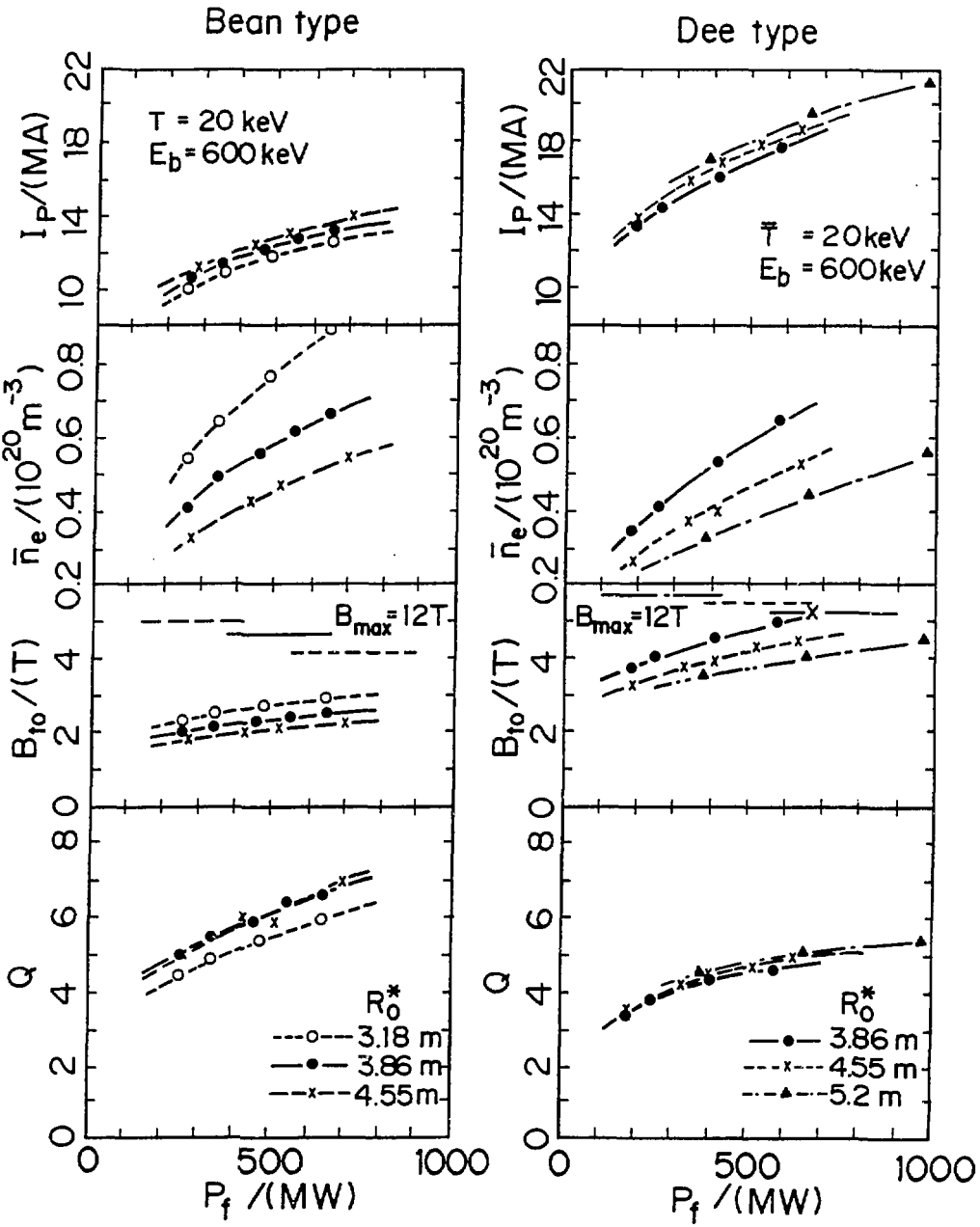
Bean type
Dee type
T = 20 keV
E_b = 600 keV
T̄ = 20keV
E_b = 600keV
I_P/(MA)
n̄_e/(10^20 m^-3)
B_max=12T
B_to/(T)
Q
R*_0
3.18 m
3.86 m
4.55m
3.86 m
4.55 m
5.2 m
P_f /(MW)
0
500
1000

Fig. 7

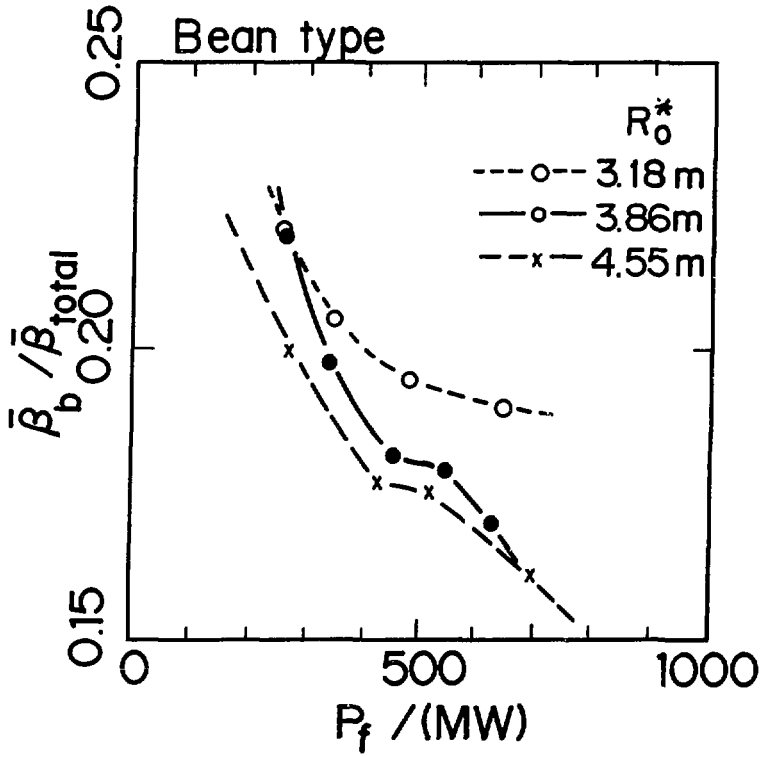
Bean type
R_0^*
3.18 m
3.86m
4.55m
$\bar{\beta}_b / \bar{\beta}_{total}$
0.25
0.20
0.15
0
500
1000
P_f /(MW)

Fig. 8

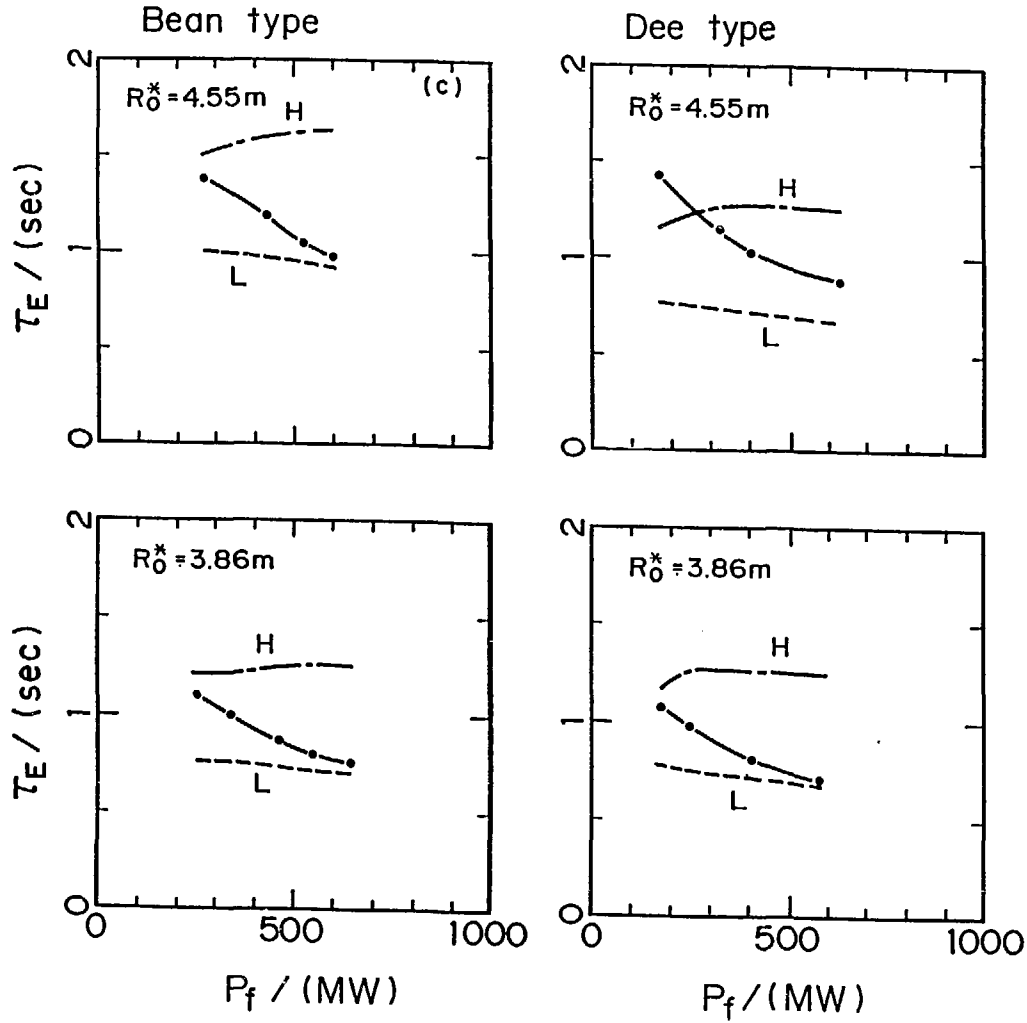
Bean type
Dee type
(c)
R_0^*=4.55m
R_0^*=3.86m
H
L
τ_E / (sec)
P_f / (MW)
0
1
2
500
1000

Fig. 9

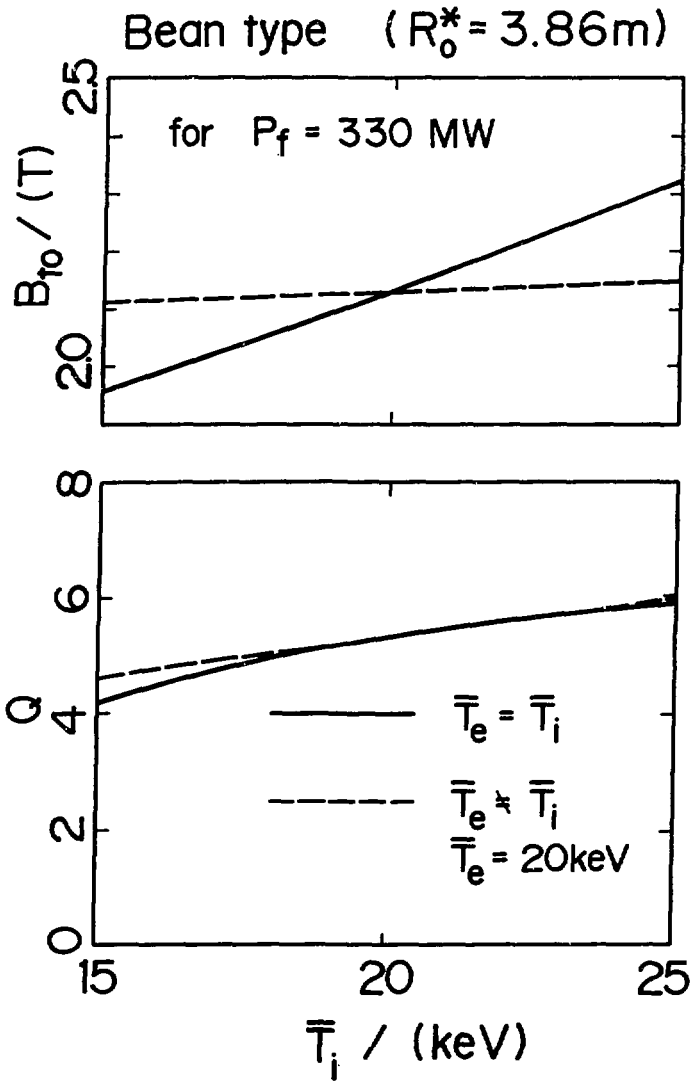
Bean type ($R_0^* = 3.86$m)
for P_f = 330 MW
B_{to} / (T)
2.5
2.0
Q
8
6
4
2
0
$\bar{T}_e = \bar{T}_i$
$\bar{T}_e \neq \bar{T}_i$
$\bar{T}_e$ = 20keV
15
20
25
$\bar{T}_i$ / (keV)

Fig. 10

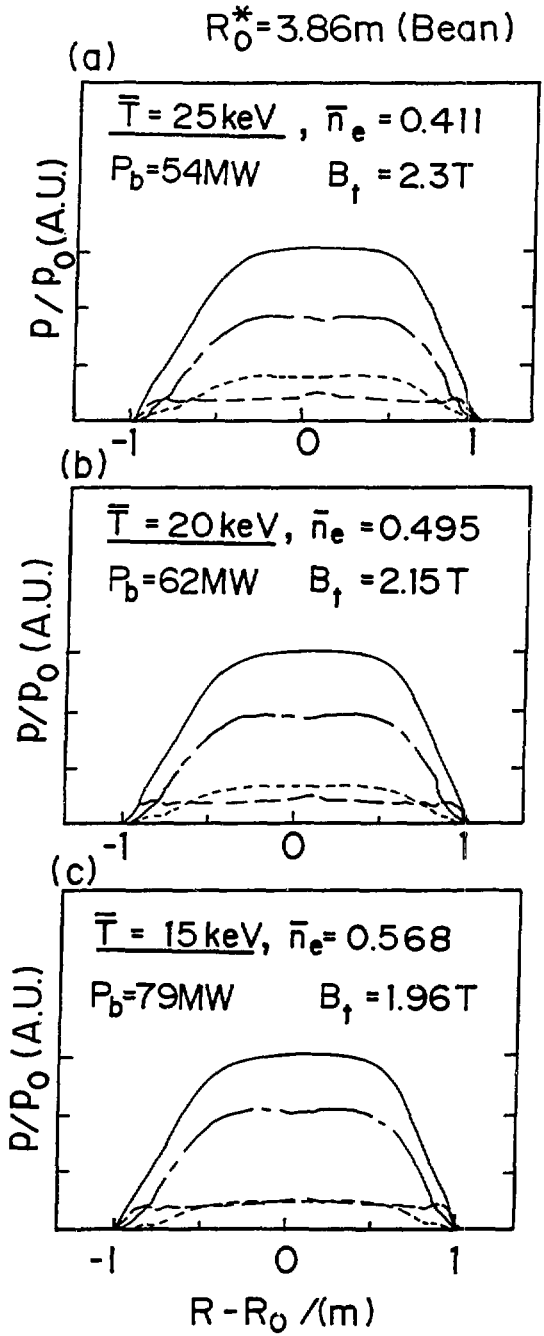
R_0^*=3.86m (Bean)
(a)
$\bar{T}$ = 25keV , $\bar{n}_e$ = 0.411
P_b=54MW B_t = 2.3T
P / P_0(A.U.)
-1
0
1
(b)
$\bar{T}$ = 20keV, $\bar{n}_e$ = 0.495
P_b=62MW B_t = 2.15T
P/P_0 (A.U.)
-1
0
1
(c)
$\bar{T}$ = 15keV, $\bar{n}_e$= 0.568
P_b=79MW B_t = 1.96T
P/P_0 (A.U.)
-1
0
1
R - R_0 /(m)

Fig. 11

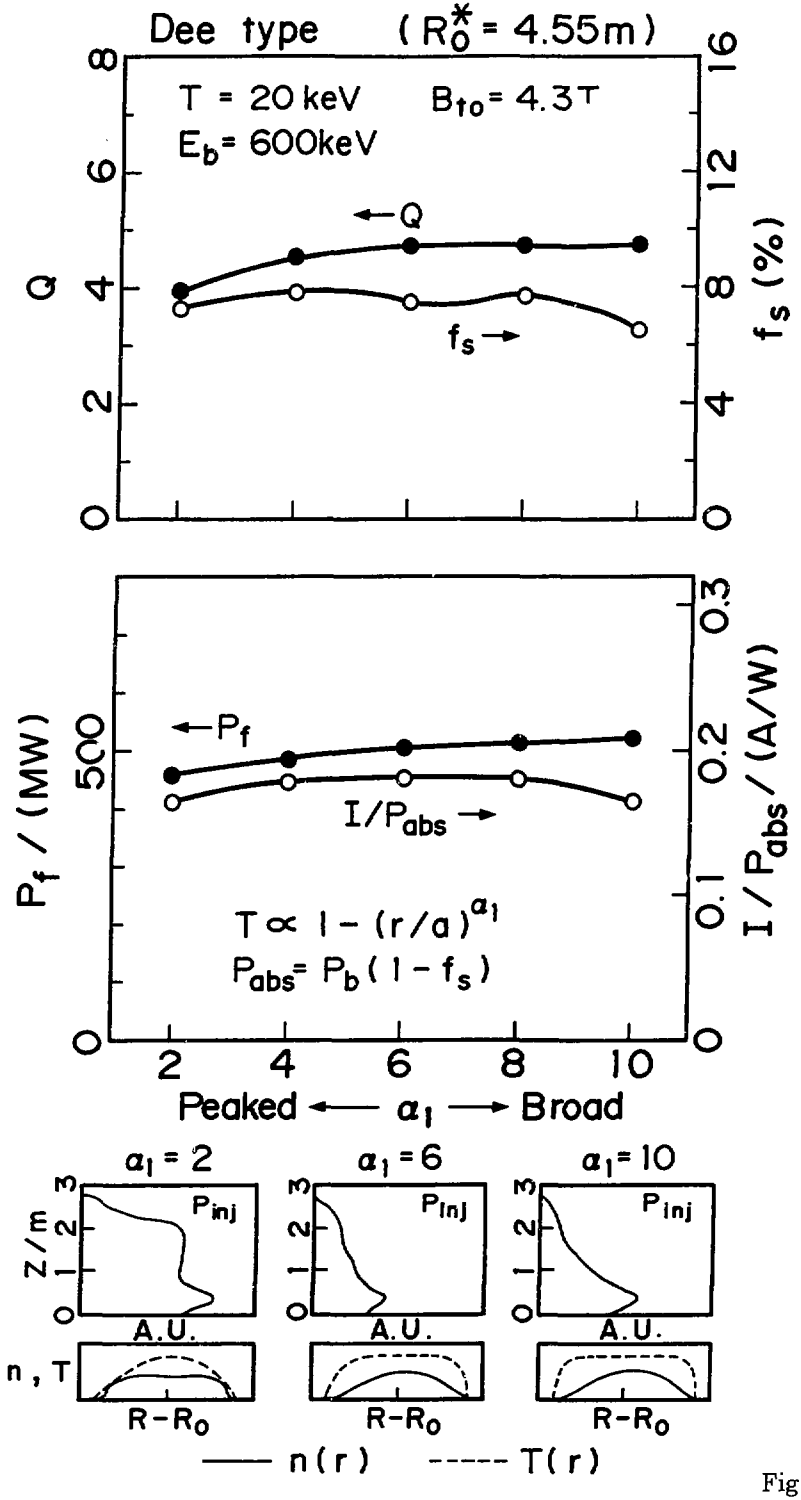
Dee type ($R_0^* = 4.55m$)
T = 20 keV
$B_{to} = 4.3T$
$E_b = 600keV$
Q
f_s
f_s (%)
P_f
P_f / (MW)
I/P_{abs}
I / P_{abs} / (A/W)
$T \propto 1 - (r/a)^{\alpha_1}$
$P_{abs} = P_b (1 - f_s)$
Peaked ← α_1 → Broad
$\alpha_1 = 2$
$\alpha_1 = 6$
$\alpha_1 = 10$
P_{inj}
Z/m
A.U.
n , T
R-R0
—— n(r) ----- T(r)

Fig. 12

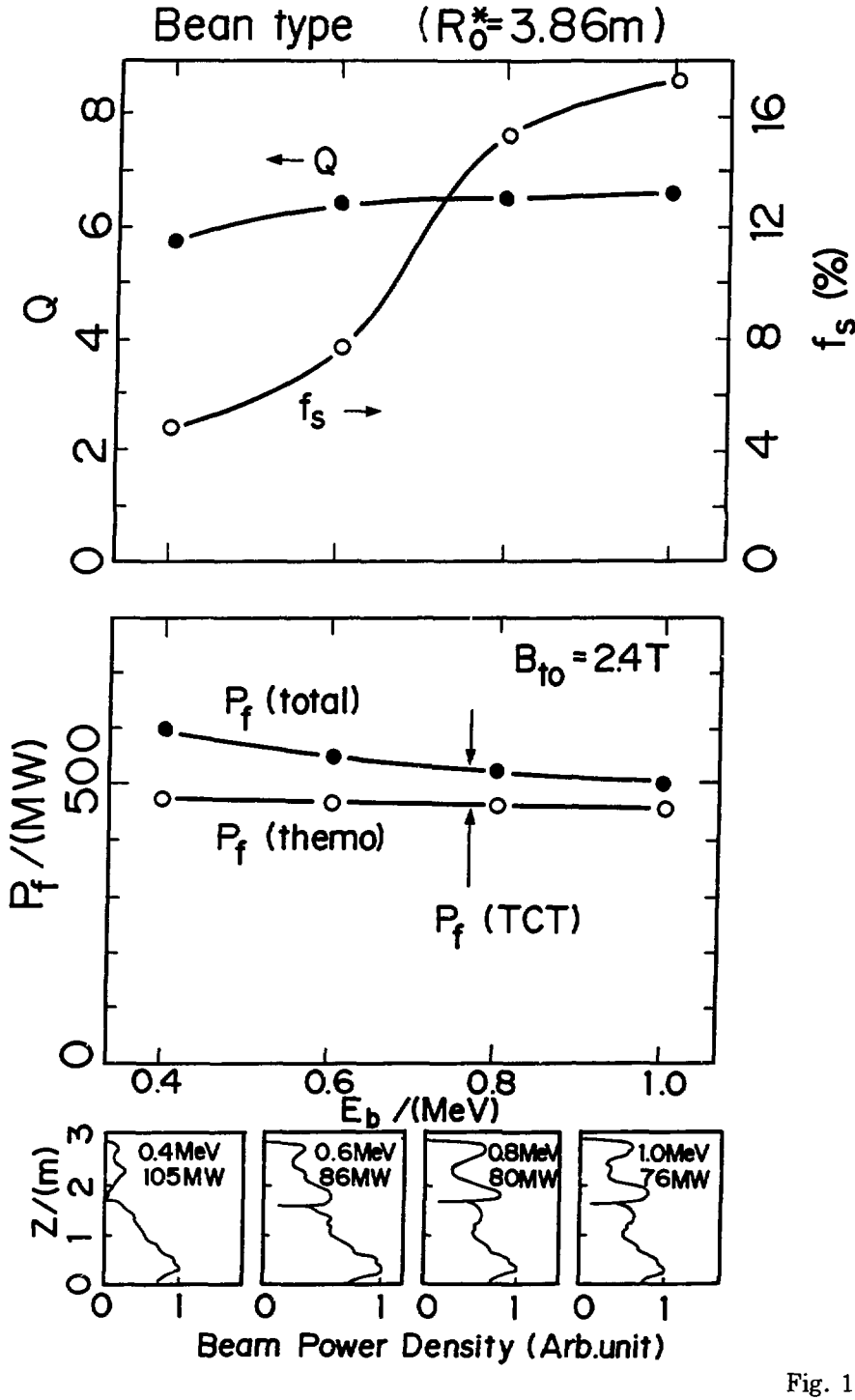
Bean type (R*0=3.86m)
Q
fs (%)
fs
Bto=2.4T
Pf (total)
Pf (thermo)
Pf (TCT)
Pf /(MW)
Eb /(MeV)
0.4MeV 105MW
0.6MeV 86MW
0.8MeV 80MW
1.0MeV 76MW
Z/(m)
Beam Power Density (Arb.unit)

Fig. 13

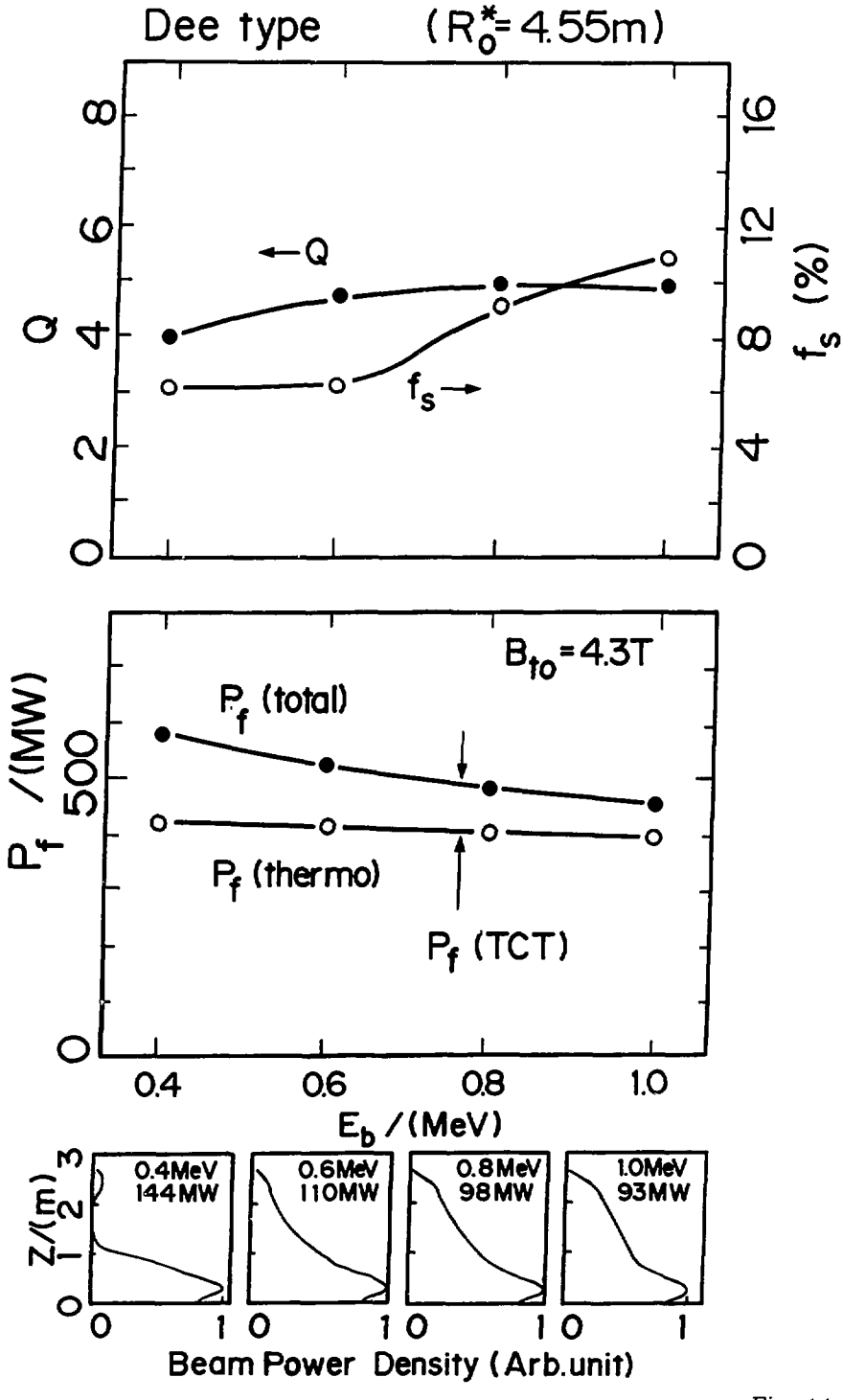
Dee type
(R_0^*= 4.55m)
Q
f_s (%)
←Q
f_s→
B_{to}=4.3T
P_f (total)
P_f (thermo)
P_f (TCT)
P_f /(MW)
E_b /(MeV)
0.4MeV
144MW
0.6MeV
110MW
0.8MeV
98MW
1.0MeV
93MW
Z/(m)
Beam Power Density (Arb.unit)

Fig. 14

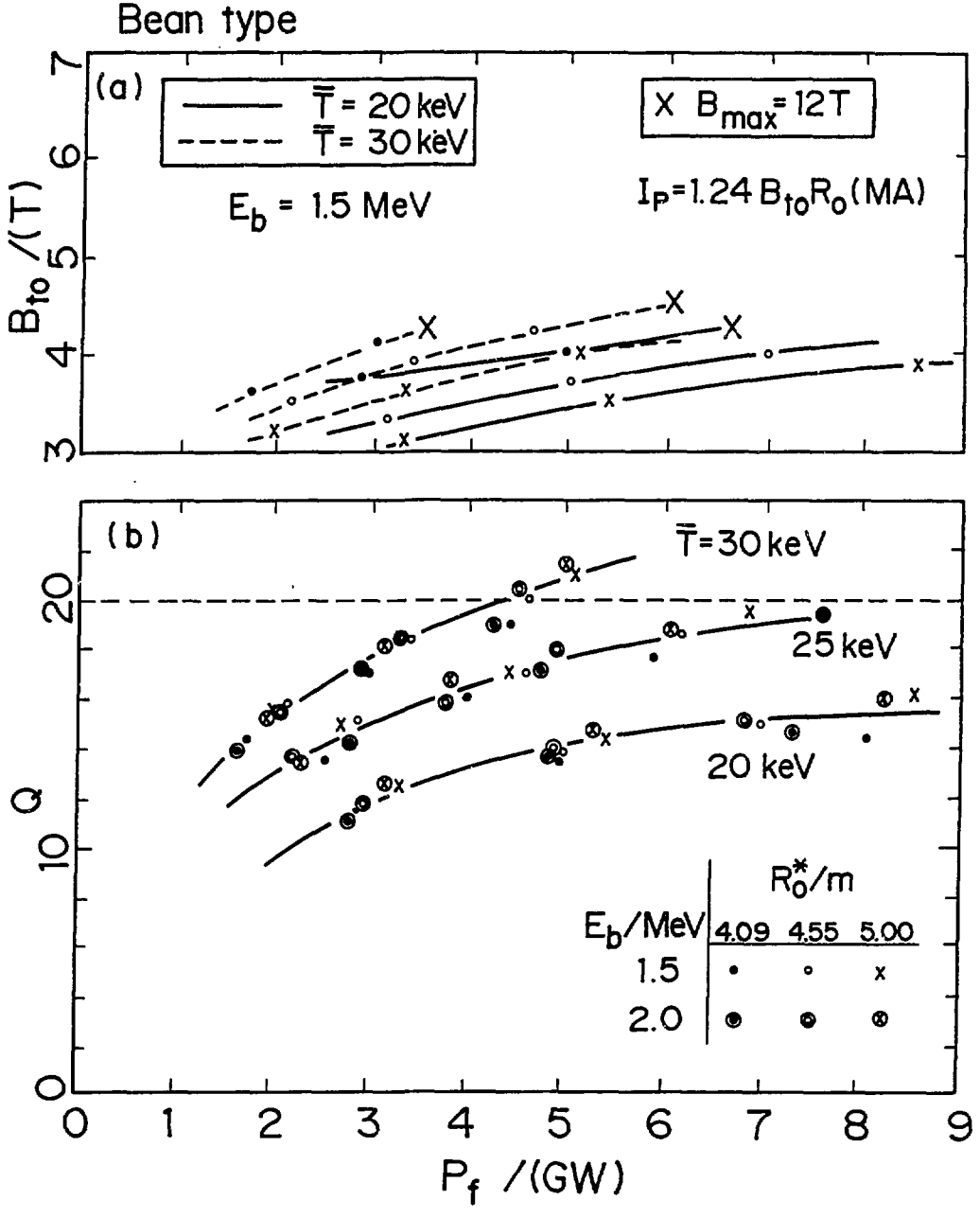
Bean type
(a)
$\bar{T}$ = 20 keV
$\bar{T}$ = 30 keV
E_b = 1.5 MeV
X B_{max} = 12T
I_P = 1.24 $B_{to} R_o$ (MA)
B_{to} /(T)
(b)
$\bar{T}$ = 30 keV
25 keV
20 keV
Q
R_o^*/m
E_b/MeV
4.09 4.55 5.00
1.5
2.0
P_f /(GW)

Fig. 15

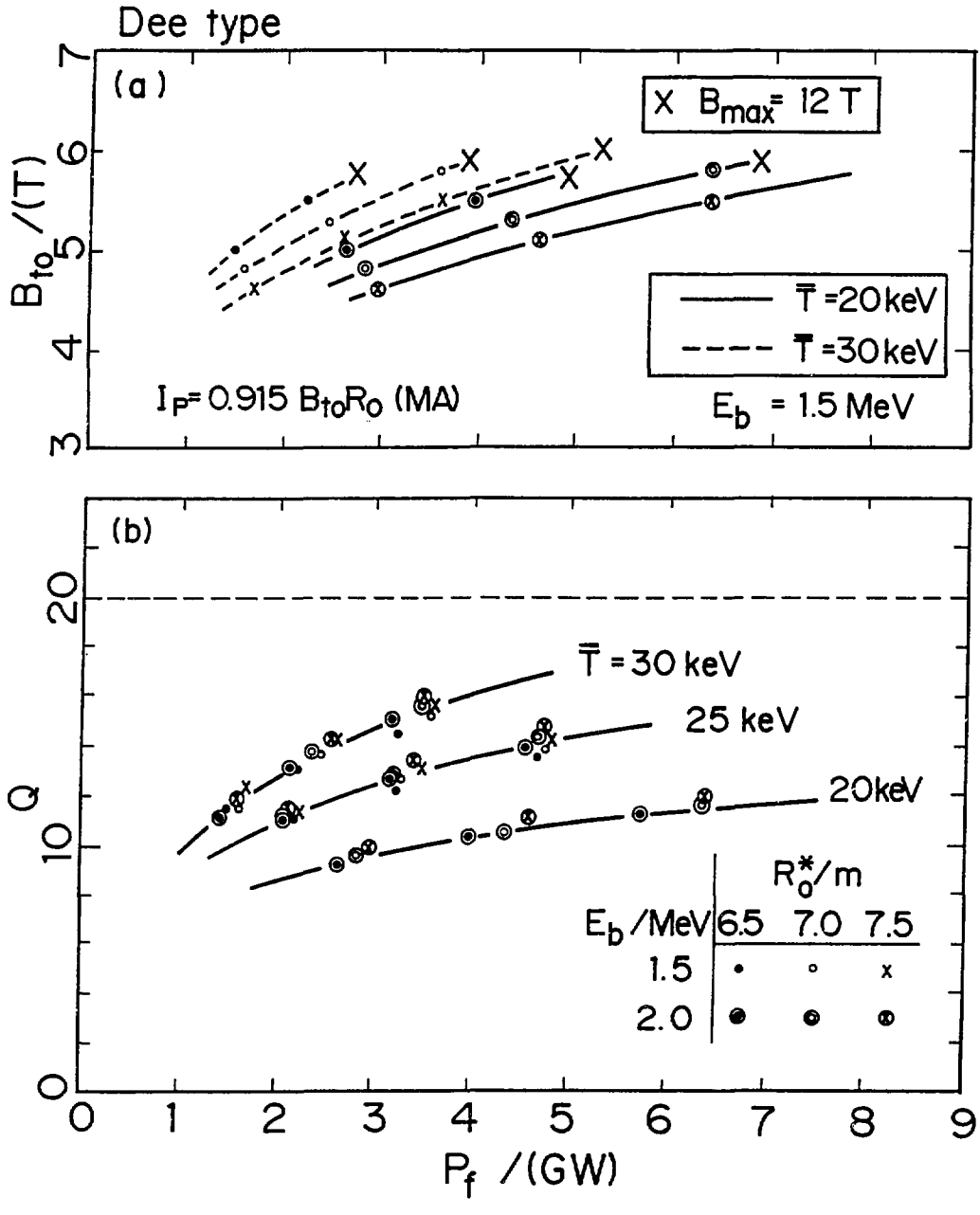
Dee type
(a)
X B_{max}= 12 T
B_{to}/(T)
$\bar{T}$ =20keV
$\bar{T}$ =30keV
I_P= 0.915 $B_{to}R_0$ (MA)
E_b = 1.5 MeV
(b)
Q
$\bar{T}$ = 30 keV
25 keV
20keV
R_0^*/m
E_b/MeV 6.5 7.0 7.5
1.5
2.0
P_f /(GW)

Fig. 16

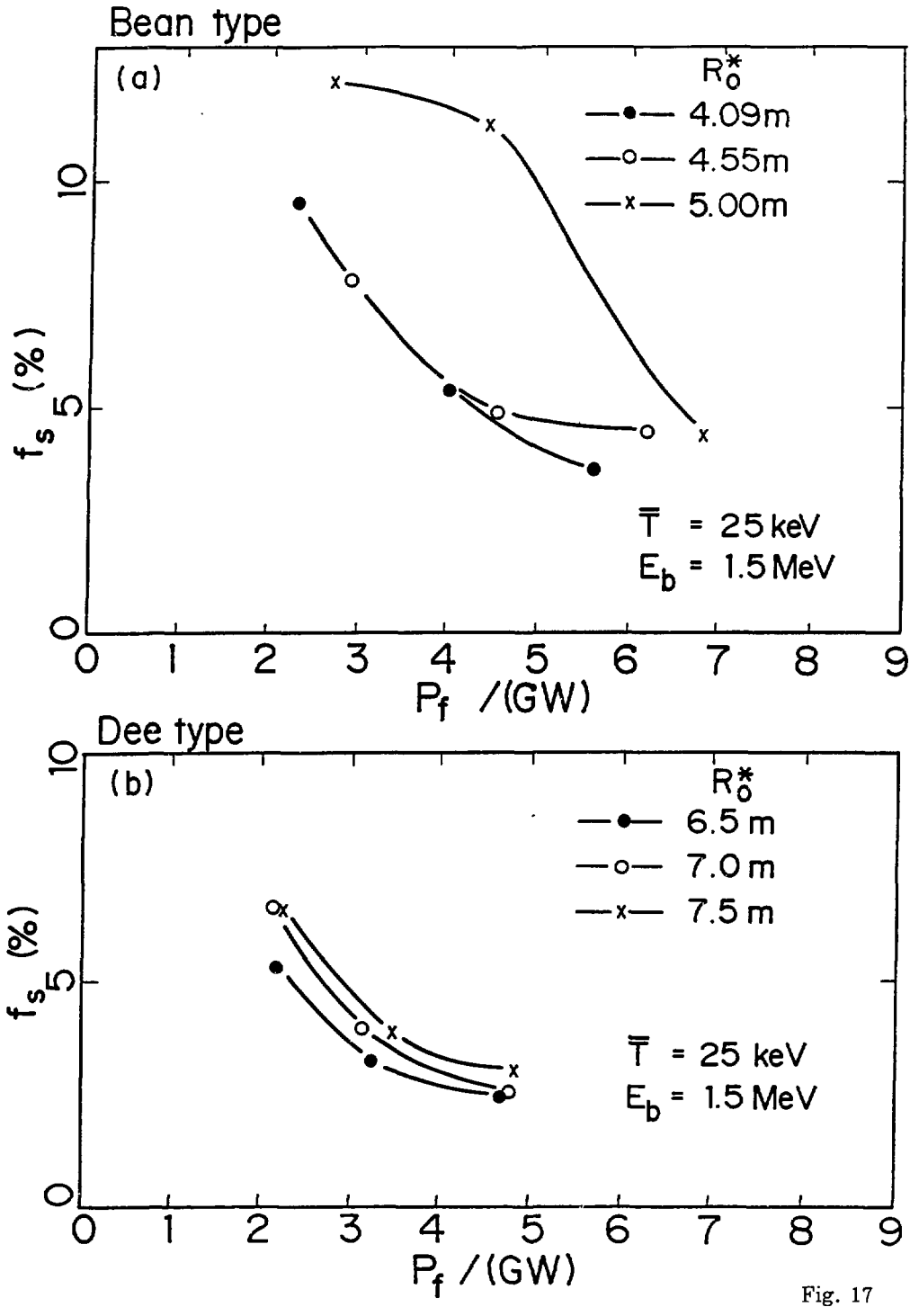
Bean type
(a)
R_0^*
4.09m
4.55m
5.00m
$\bar{T}$ = 25 keV
E_b = 1.5 MeV
f_s (%)
P_f /(GW)
Dee type
(b)
R_0^*
6.5 m
7.0 m
7.5 m
$\bar{T}$ = 25 keV
E_b = 1.5 MeV
f_s (%)
P_f /(GW)

Fig. 17